Master Thesis

Fabrication of dye-sensitized solar cells using natural dyes extracted from Brazilian plants

Marcelo Alatzatianou Rodrigues

University of Freiburg, Germany
Faculty of Engineering
Department of Microsystems Engineering (IMTEK)

Submitted as part of the Master Program
"Solar Energy Engineering"

May 2020

This is a Master Thesis submitted in fulfillment of the requirements for the degree of Master of Science in Photovoltaics according to the examination regulations at the University of Freiburg.

Author	Marcelo Rodrigues
	Rua Francisco de Vitória, 145
	São Paulo, SP, Brasil
	alatza@gmail.com

Thesis Period	November 1st, 2019–May 4th, 2020
First Examiner	Prof. Dr. Ricardo Rüther
Second Examiner	Prof. Dr. Stefan Glunz
Scientific Supervisor	Prof. Dr. Ricardo Rüther

DECLARATION

I hereby declare, that I am the sole author and composer of my Thesis and that no other sources or learning aids, other than those listed, have been used. Furthermore, I declare that I have acknowledged the work of others by providing detailed references of said work.

I hereby also declare, that my Thesis has not been prepared for another examination or assignment, either wholly or excerpts thereof.

_____ _____

Place, date Signature

Acknowledgements

Thanks for the many people who contributed to make this work possible, with special thanks to the following incredible people.

Prof. Stefan Glunz, for the open-minded view when giving the opportunity for the student follows the heart on choosing the subject for the thesis.

Prof. Ricardo Rüther, for the support and guidance.

Philipp Bucher, for the incredible support and amazing dedication on every aspect of the Master program.

Prof. Uli Würfel, for being an inspiration, for simplifying what seems too complex, for being available, and for the amazing opportunity of learning beyond the program.

Luis del Águila Escamilla, for the patience and many hours of detailed explanations on laboratory practice.

Prof. Martin Heinrich, for opening doors, inspiring and show the way.

Barbara Gumbert, for the noble efforts in making things happen.

My student colleagues, for sharing their life experiences and energy.

Special thanks to Domingos Sávio Rodrigues, director of Jardim Botânico de São Paulo, for the amazing support.

Zusammenfassung

Die farbstoffsensibilisierte Solarzelle (DSSC) ist eine der aufkommenden Dünnschicht-Photovoltaik-Technologien. Vorteile ergeben sich aus den geringen Kosten und dem einfacheren Herstellungsprozess. Die realistische Gesamtumwandlungseffizienz hat die kommerzielle Verfügbarkeit bereits Wirklichkeit werden lassen.

Es ist möglich, natürliche Farbstoffe zu verwenden, die bei der DSSC-Herstellung aus Pflanzen extrahiert werden, um synthetische Farbstoffe zu ersetzen, was komplexe Herstellungsprozesse und die Verwendung toxischer und seltener Materialien wie Ruthenium erfordert. Natürliche farbstoffsensibilisierte Solarzellen (NDSSC) befinden sich noch in einem frühen Stadium. Viele Forschungsgruppen arbeiten hart daran, Effizienz- und Stabilitätsprobleme zu überwinden. Natürliche Farbstoffe sind billig, hochverfügbar, umweltfreundlich und leicht zu extrahieren.

Die Natur hat der Menschheit so viel zu bieten, dass jede Pflanze einzigartig ist und Eigenschaften aufweist, die sich in Millionen von Jahren der Evolution entwickelt haben. Jedes Biom verfügt über eine enorme Anzahl von Arten, die für Studien zur Verfügung stehen. Unter ihnen befinden sich brasilianische Wälder in einer hervorragenden Position mit einer riesigen Menge von Arten mit versteckten Möglichkeiten.

Diese Arbeit soll andere Forscher dazu inspirieren, dieses Gebiet zu erkunden und in der Natur neue Antworten für eine Welt zu finden, die saubere Energie erfordert. Es werden die grundlegenden Aspekte der NDSSC-Studie und der praktischen Forschung gezeigt, vom Laboraufbau bis zur Zellherstellung.

Nach einer kurzen Einführung in PV-Technologien wird DSSC anhand einer Literaturübersicht eingehender erörtert. Physikalische und elektrochemische Aspekte werden detailliert dargestellt. Die Spezifitäten und Anwendungen natürlicher Farbstoffe in DSSC werden dann auch auf der Grundlage anderer Forscherergebnisse diskutiert.

Mit einer gut etablierten theoretischen Grundlage konzentriert sich diese Arbeit dann auf die Entwicklung eines NDSSC-Herstellungsprotokolls, in dem die wichtigsten erzielten Tests und Ergebnisse vorgestellt werden. Ein besonderes Highlight ist das Design und die Herstellung eines Solarsimulators von Grund auf neu.

Nachdem die Infrastruktur, die Ausrüstung und das Protokoll definiert waren, war die Herstellung von NDSSC auf der Basis brasilianischer Pflanzen möglich, einschließlich Pflanzen, die ihren natürlichen Ursprung im Land haben: Brombeere, Quaresmeira und Embaúba-Vermelha sowie zwei weitere nicht heimische Arten aufgrund ihrer wirtschaftlich wichtigen Rolle. Davon ist Brasilien derzeit der weltweit führende Produzent: Arabica-Kaffee und Zuckerrohr.

Die gefundenen Zelleffizienzen für alle untersuchten Pflanzenfarbstoffe liegen im Bereich anderer wichtiger Forschungspublikationen, selbst für das vereinfachte und kostengünstige

vorgeschlagene Protokoll, das die verwendeten Lösungen und Techniken validiert.

Coffea arabica (Arabica-Kaffee) lieferte die beste Leistung und erreichte eine Gesamtumwandlungseffizienz von 0,44% ohne spezielle, üblicherweise verwendete chemische Behandlung, Co-Adsorbens oder Reinigung wie $TiCl_4$, organische Säuren, Chromatographie und Gefriertrocknung.

Es ist zu hoffen, dass diese Arbeit zur Entwicklung einer noch umweltfreundlicheren Energieerzeugung aus Sonnenlicht beiträgt.

Abstract

Dye-sensitized solar cell (DSSC) is one of the emerging thin-film photovoltaic technologies. Advantages come from the low cost and easier fabrication process. The realistic overall conversion efficiency already made the commercial availability a reality.

It is possible the use of natural dyes extracted from plants in DSSC fabrication to substitute synthetic dyes, which requires complex fabrication processes and the use of toxic and scarce materials, like ruthenium. Natural dye-sensitized solar cells (NDSSC) are still in an early stage, with many research groups working hard to overcome efficiency and stability issues. Natural dyes are cheap, highly available, environmentally safe and easy to extract.

Nature has so much to offer to humankind, each plant is unique, with characteristics developed during million of years of evolution. Each biome has an enormous number of species readily available for study. Among them, Brazilian forests are in an outstanding position, with a gigantic quantity of species with hidden opportunities.

This work aims to inspire other researchers to explore this field and find in nature new answers for a clean energy demanding world. It is shown the basic aspects of NDSSC study and practical research, from laboratory construction to cells fabrication.

After a brief introduction about PV technologies, DSSC is deeper discussed based on a literature review. Physical and electrochemical aspects are presented in details. Natural dyes specificities and application in DSSC are then discussed also based on other researchers findings.

With a well-established theoretical basis, this work focus then on the development of a NDSSC fabrication protocol, presenting the most important tests and results achieved. A special highlight is given to the design and fabrication of a solar simulator from scratch.

Having the infrastructure, equipments and protocol defined, the fabrication of NDSSC based on Brazilian plants was possible, including plants naturally originated in the country: blackberry, quaresmeira and embaúba-vermelha, and two other non-native species due to their economically important role, of which Brazil is currently the world leader producer, they are: arabica coffee and sugarcane.

The found cells efficiencies for all studied plants dyes are in the range of other important research publications, even for the simplified and low cost proposed protocol, which validates the solutions and techniques used.

Coffea arabica (arabica coffee) provided the best performance, reaching 0.44% overall conversion efficiency, with no special commonly used chemical treatment, co-adsorbent or purification, such as: $TiCl_4$, organic acids, chromatography and lyophilization.

It is hoped this work contribute for the development of an even greener energy generation from sunlight.

Table of Contents

1. Introduction

1.1. Photovoltaic energy

Among the available renewable energy sources, sunlight is available everywhere. There is no location in the world lacking of it. Among solar irradiance harvesting technologies, photovoltaic (PV) exhibits important characteristics which make it one of the most important global electricity generation solutions. PV, specially based on crystalline silicon, is already very mature and scalable [1], with costs dropping and installed power growing very fast [2].

Nevertheless, PV is not restricted to panels made of crystalline silicon solar cells. To achieve further costs reduction, increasing efficiency and finding new utilization possibilities, researchers all around the world have dedicated efforts to find new ways to generate electricity from sunlight and have created several PV technologies based on different materials with creative structures and clever working principles.

1.2. Main PV technologies briefly

Jean et al. [1] classified the different PV technologies in 2 groups: wafer and thin film. Crystalline silicon (c-Si) wafer-based solar cells are fabricated by cutting slices from a silicon cast block (multi-crystalline) or from a silicon grown ingot (mono-crystalline or single-crystalline). Solar cells are then made by modifying the wafer with several processes (doping, texturing, metallization, etc).

Crystalline silicon wafer-based solar cells are the dominant technology in the market [2]. The stability and high efficiency achieved, along with very well-established industrial processes, make this technology affordable and very advantageous.

Thin film-based solar cells (TF) fabrication usually involves the deposition of layers of semiconductor materials on a substrate like glass, metal or even plastic. The deposition usually requires complex and expensive chemical or physical vapor depositions, although solution-based processes are also viable. TF require very thin layers of semiconductor material due its usually high light absorbance. This advantage offers the opportunity to use less material and fabricate flexible panels, well suited for many applications where c-Si are not appropriate.

As a subdivision, Jean et al. [1] proposes 2 TF groups: commercial thin film and emerging technologies. The first is composed of the technologies already being commercialized in the market. The authors also describe some important facts of each technology as follows.

Hydrogenated Amorphous Silicon (a-Si:H), usually deposited by plasma-enhanced chemical vapor deposition (PECVD), the amorphous silicon film exhibits stronger absorption, although the band gap does not match the solar spectrum.

Cadmium Telluride (CdTe) is the market leading technology, with record efficiencies of 21% for cells and 17.5% for panels. The cadmium toxicity is a big concern.

Copper Indium Gallium Diselenide (CIGS) can be deposited by a variety of techniques, including solution and vapor-based, over flexible substrates, which makes this technology favorable for building integration.

Due to the effort of researchers all around the world to find new options which may offer better efficiencies, ease of fabrication, lower costs and environmental safety, new emerging technologies has been developed.

Perovskite. The term refers to an ABX_3 crystal structure. Among the advantages of this material are the carrier long diffusion lengths, low recombination losses and band gap tunability. Efficiencies of this kind of cells overcome 20% in just the first years of research, which perhaps makes it the most promising emerging technology, although the devices stability is still a concern.

Organic Photovoltaics (OPV). Despite efficiencies just above 10%, this alternative is very interesting due to the possibility of high-throughput deposition methods used, such as roll-to-roll fabrication. The utilized materials are small molecules and polymer-based.

Quantum-dot photovoltaics (QDPV). Consisting of solution-processed nano crystals, QDPV brings the opportunity of tuning band gap by the crystal size. This characteristic can be used to create multi-junction cells, closer matching the solar irradiance spectrum.

Dye-sensitized solar cells (DSSC), is another important technology. However, since it is the subject of the present work, a more detailed introduction will be presented in the next section.

National Renewable Energy Laboratory (NREL) maintains a chart of the research solar cells with the best confirmed efficiencies by year since 1976 [3], this is an important reference for technologies comparison.

1.3. Dye-sensitized solar cell

Dye-sensitized solar cell (DSSC) is one of the most mature technology listed among the emergent alternatives, even though it is already commercially available. Unlike the others, this technology uses liquid electrolyte, although all-solid or quasi-solid states have been also developed. Cell record efficiency is now 12.6% [3]. DSSC exhibits lower efficiency, if compared with crystalline silicon cells or some other emerging technologies. Challenges are also related to long term stability and electrolyte leakage. On the other hand, DSSC benefits from easy and low cost fabrication processes, good efficiency under diffuse and low light intensities, colorful final products and flexible substrates, advantages for buildings integration [4][5][6].

DSSC light harvesting is essentially based on light absorption by molecules of dyes anchored to the surface of a semiconductor mesoporous layer, usually nano particles of TiO_2

[7]. Those dyes are commonly made of synthetic, rare and toxic materials based on ruthenium (Ru), but they can be replaced by plants pigments, which are eco-friendly, low cost, simply extracted and widely available, despite of their still low efficiency and stability [4]. Those DSSC made of natural dyes are often called natural dye-sensitized solar cells (NDSSC).

Iqbal et al. [8] in their 2019 review brought several published works exhibiting NDSSC efficiencies between 1% and 2%, although most of the publications are still below this range. Exceptionally, Sanjay et al. [9] could reach 8.22% efficiency from cells made with *A. amantacea* and *P. pterocarpum* leaves in ethanol.

1.4. Present work goals

Considering the early stage of NDSSC which offers interesting research challenges, also the promising contribution of this technology for humankind and the planet, the present work aimed to reach the following goals:

1. Establish a new laboratory for DSSC research and education.
2. Present and encourage the use of NDSSC as an entrance gate to the PV world for new researchers and institutions.
3. Develop a low cost, simple and reliable fabrication protocol for NDSSC.
4. Contribute with NDSSC research presenting details and results on the use of some Brazilian plants.

As Kumara et al. [4] stated, the low entry cost of DSSC fabrication was the motivation for their review work: “This means laboratories with the basic equipment and know-how could technically produce a laboratory level cell”. With this point of view in mind, the present work is developed. Learning from the available literature and several experiments, the goal was to reach a technical level high enough to contribute to the PV scientific community, maybe also inspiring new researchers to find their own ways to contribute to the clean energy world.

At the same time, the present work will focus on the use of natural dye-sensitized solar cells (NDSSC) using dyes extracted from Brazilian plants. Brazilian biodiversity offers an uncountable number of the plants species, each of them with specific solutions for their ecosystems challenges for survival. Evolution made its work in each of them, through millions of years of variation and adaptation, optimizing and differentiating their biochemistry.

1.5. Document organization

For a better reading experience, this work is organized as follows:

Section 1 presents this work motivation and goals.

Sections 2, 3 and 4 bring the theory behind the technology and the knowledge provided by several publications.

Section 5 presents the fabrication protocol development process, including experiments (simplified batches), considerations and decisions taken. The section ends with the complete suggested fabrication protocol, including materials and equipments.

Section 6 brings the results obtained by the cells fabricated using dyes extracted from the selected Brazilian plants.

Section 7 offers final considerations.

Section 8 lists all references.

2. Literature Review

DSSC history started more than one century ago, through experiments with silver halide in 1870 by Vogel et al. Other discoveries and understanding of the principles of dye generation of carriers and transport were achieved from the contribution of several researchers [4].

However, until 1991, DSSC exhibited prohibitive efficiencies, lower than 1%. In that year, O' Regan and Grätzel presented a DSSC based on mesoporous layer of TiO_2 nanoparticles sensitized by a trimeric ruthenium complex, which achieved 7.1% efficiency in full light and 12% in diffuse light [7]. In the authors words: "Because of the high surface area of the semiconductor film and the ideal spectral characteristics of the dye, the device harvests a high proportion of the incident solar energy flux (46%) and shows exceptionally high efficiencies for the conversion of incident photons to electrical current (more than 80%)".

Because of Grätzel contributions since the late 1980s to the development of DSSC, this cell structure is also known as Grätzel cell.

2.1. DSSC working principle

DSSC construction diagram can be seen in Figure 2.1 [7][5][6]. The cell is made of 2 main parts, a photoanode (left side) and a cathode (right side), with an usually liquid electrolyte in the middle (yellow area).

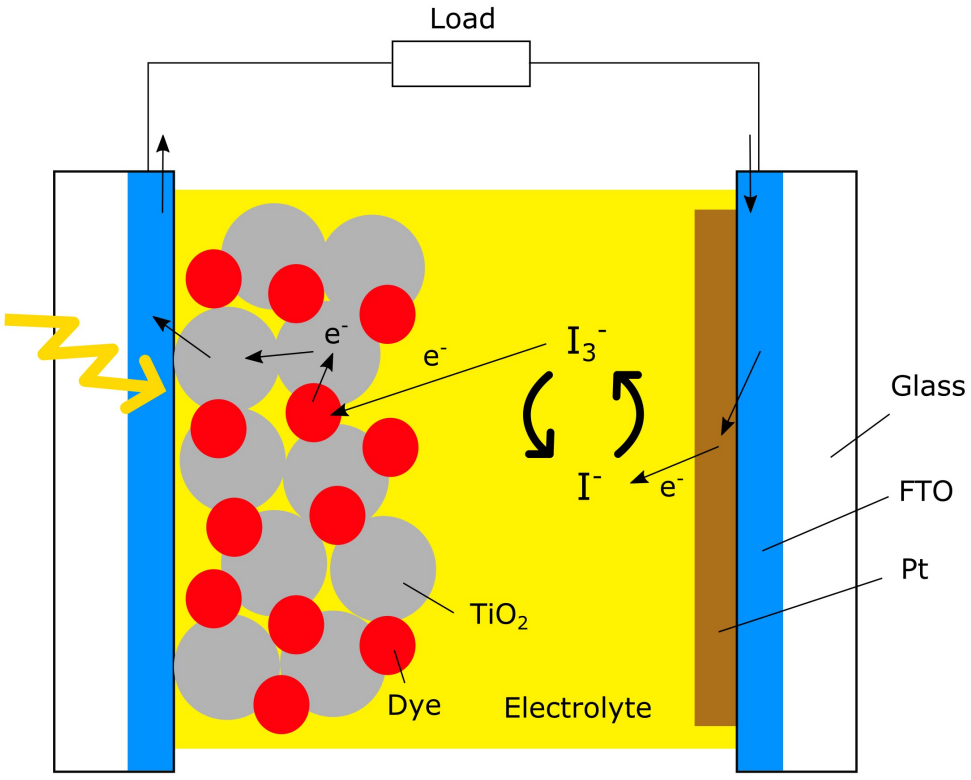

Figure 2.1: Construction diagram and working principle of a DSSC.

The photoanode is a piece of glass with a conductive coating of TCO (transparent conductive oxide) on one side (blue area), under a deposition of a thin layer of mesoporous semiconductor, formed by a network of TiO_2 nanoparticles (gray circles) with an internal surface of about 1000 cm^2 per 1 cm^2 [4]. When immersed in a dye solution the dye molecules (red circles) are adsorbed by the TiO_2 network internal surface, creating an enormous light harvesting surface [7][5].

Similar to the photoanode, the cathode is another piece of glass with a TCO covering on one side (blue), over it a catalytic layer is deposited, usually platinum or carbon (brown area) [5].

Photoanode and cathode are externally connected to a load, via metal contacts (black lines on the upper part of Figure 2.1).

Below, the working principle of DSSC will be explained. Figure 2.1 and Table 2.1, which contains the chemical equations referenced in the text, can be used for a better understanding of the events.

Everything starts when a photon (represented by the yellow arrow in Figure 2.1) hits a dye molecule. If the photon has enough energy, the dye molecule will be excited (equation I in Table 2.1). Due to energetic and entropic driving forces in the dye/TiO_2 interface [10], the excited dye molecule then injects an electron on the TiO_2 conduction band keeping a hole charge carrier (equation 2). The free electron moves through the TiO_2 particles surface network [10] and finds its way out of the device via the photoanode TCO and external metal contact. As explained by O' Regan and Grätzel [7]: “Dye-sensitized cells differ from the conventional semiconductor devices in that they separate the function of light absorption from charge carrier transport”.

Work is done in the load and the electron returns via cathode metal contact and TCO until reaching the catalytic layer, which forms an interface with the electrolyte.

The electrolyte is made of a redox couple, usually I^-/I_3^-. In the presence of the catalyst, I_3^- ions are reduced to I^- (equation III) and can rearrange (not move [10]) towards the oxidized dye to regenerate to its relaxed state (equation IV) and thus, finishing the cycle.

Photoexcitation	$Dye\ (on\ TiO_2) + h\nu \rightarrow Dye^*\ (on\ TiO_2)$	(I)
Charge Injection	$Dye^*\ (on\ TiO_2) \rightarrow Dye^+\ (on\ TiO_2) + e^-\ (on\ TiO_2)$	(II)
Reduction	$I_3^- + 2e^-\ (on\ Pt) \rightarrow 3I^-$	(III)
Regeneration	$2Dye^+\ (on\ TiO_2) + 3I^- \rightarrow 2Dye\ (on\ TiO_2) + I_3^-$	(IV)

Table 2.1: Main chemical reactions occurring in DSSC (excluding loss processes) [8][4].

The cycle presented above would be an ideal situation. Unfortunately, at the same time, other reactions occur in the cell, those reactions are loss mechanisms which reduce the cell performance [11].

Table 2.2 lists the main loss reactions. Equation V represents the recombination of the oxidized dye directly with electrons on the TiO_2. Those electrons are then lost without contributing to the external electric current. Besides, the same electrons on TiO_2 may react with the electrolyte I_3^- ions, also causing loss, as represented in equation VI. Furthermore, dye molecules may relax from the excited state before the injection of an electron into TiO_2 occurs (equation VII).

Recombination	$Dye^+ (on\ TiO_2) + e^- (on\ TiO_2) \rightarrow Dye\ (on\ TiO_2)$	(V)
Recombination	$2e^- (on\ TiO_2) + I_3^- \rightarrow 3I^-$	(VI)
Relaxation	$Dye^* (on\ TiO_2) \rightarrow Dye\ (on\ TiO_2)$	(VII)

Table 2.2: Main loss reactions occurring in DSSC [8][4].

Those loss reactions should be avoided as much as possible, choosing the right materials and fabrication processes which make the DSSC working cycle reactions faster and much more probable. Thus, researchers must consider all these events during design and fabrication.

Materials selection takes into account several characteristics, but the energy levels of each material are one of the most important factors. They will define how fast the carriers can pass through each interface and reduce the probability of loss mechanisms to happen. For each interface there is a driving force caused by the difference of fermi levels of each material [10]. It is interesting to add that since there is no minority carriers involved, surface and bulk recombination losses due to lattice defects, as encountered in conventional photovoltaic cells, are not observed in DSSCs [7].

Figure 2.2 shows the energy levels diagram of the same ideal cell explained above [7] [5][11]. Each reaction in Table 2.1 is also represented. The chosen colors correspond to the same parts presented in Figure 2.1 for easy correspondence.

As mentioned in the previous section, ruthenium (Ru) is the most common material on which synthetic dyes are based. It has been reported that the photoexcitation happens in between 100 femtoseconds (fs) to 100 picoseconds (ps), depending on experimental conditions (equation I), while the relaxation time (equation VII) occurs in about 20 nanoseconds (ns), much slower [4].

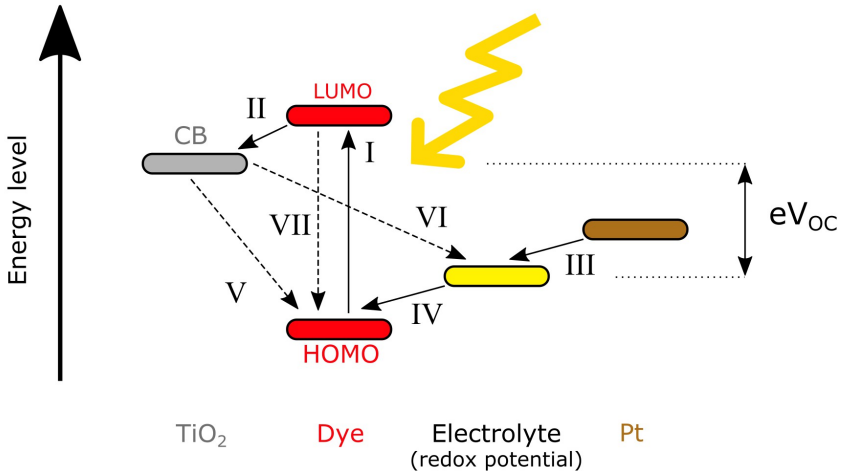

Figure 2.2: Energy levels diagram of an ideal DSSC [7][5].

The same comparison can be made between recombination processes (equations V and VI) which electrons on TiO_2 are lost due recombination with oxidized dye or electrolyte ions, and the regeneration process (equation IV), the first occur in micro to milliseconds range, while the second is faster, taking 0.1 to 10 microseconds [4].

Kumara et al. [4], conclude: "The electron injection, electron transport and dye regeneration are the three most important processes in a solar cell to be fulfilled in order to achieve reasonable efficiency".

In a simplified point of view, the overall goal is converting solar irradiance (light) to electric power, which is the product of the voltage by the current. If one puts a solar cell under sunlight and measure the voltage on its terminals, the reading on the voltmeter corresponds to V_{OC} (open circuit voltage). This potential emerges due to the increase of electrons concentration in the TiO_2 [10].

Open circuit voltage (V_{OC}) of a DSSC corresponds to the difference between the energy level of the conduction band of the TiO_2 (CB) and the redox potential of the electrolyte (I_3^-/I^-) [4][10][7]. But this value can be lower due to the recombination processes shown above. Formula 2.1 shows how V_{OC} can be expressed. It is clear how the difference of the energy level of TiO_2 conduction band (E_{CB}) and the redox potential of the redox couple (E_{REDOX}) corresponds to V_{OC}.

$$e.V_{OC} = E_{CB} + k_B.T.\ln\left(\frac{n}{N_{CB}}\right) - E_{REDOX} \quad (2.1)$$

e is the elementary charge
k_B is the Boltzmann constant
T is the temperature
n is the number of electrons in the conduction band
N_{CB} is the density of states in the conduction band

The higher the difference between the LUMO (lowest unoccupied molecular orbital) and HOMO (highest occupied molecular orbital) of the dye molecule, the higher is the possible V_{OC}, if the rest of the cell is adjusted to keep as much as possible of that potential. This difference of the LUMO and HOMO levels is also known as the band gap (Eg). It is important to understand that Eg corresponds to the minimum photon energy necessary to excite the dye, thus, if Eg is too high, only the photons with short wavelength will be absorbed and contribute to the electric current. Therefore, a balance must be done to maximize the cell output power.

The DSSC current is dependent of many factors, mainly the dye light absorption for each wavelength, electron injection efficiency from the dye to TiO_2 and redox efficiency of the electrolyte [4].

It is possible to anticipate the cell current integrating the product of IPCE(λ) and the photon flux (Is) over the incident light spectrum, as seen on formula 2.1.2. In the given formula, J_{SC} is the short circuit density, which is the short circuit current per cell area unit [4]. IPCE(λ) is the function of the incident photon to current conversion efficiency per wavelength.

$$J_{SC} = e.\int IPCE(\lambda).Is(\lambda)\,d\lambda \quad (2.2)$$

Voltage and current behavior of the cell is usually studied via mathematical models based on the cell response under different applied voltage and temperature conditions. The most used tool is the electric equivalent circuit, which will be discussed in the next section.

2.1.1. Electric parameters and equivalent circuit

Above, it was presented the physical and electrochemical aspects behind the working principle of a DSSC. Now it will be presented an outside view of the device and the main parameters of interest that can be calculated and measured through the cell metal contacts.

Han et al. [12] state “it is necessary to obtain DSC equivalent circuits to accelerate the development of practical DSC-based photovoltaic modules”. In fact, the development of NDSSC also benefits from the study of the DSSC model, so each factor can be separately

studied and optimized to reach a viable technology based on natural dyes. Han et al. [12] used electrochemical impedance spectroscopy to examine the internal resistances of DSSC and their dependence on the applied voltage. With the obtained information, the group could propose an equivalent circuit for DSSCs (Figure 2.3).

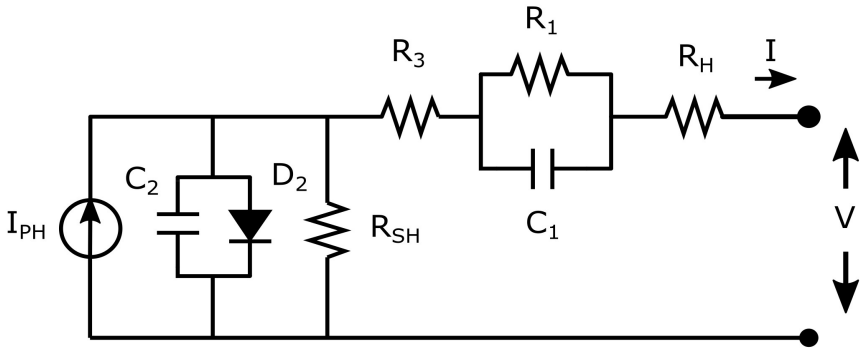

Figure 2.3: DSSC equivalent circuit obtained by Han et al. [12].

Below, in Table 2.3 all the elements in the proposed equivalent circuit are listed. This analysis is very important for a better understanding of a DSSC operation and the impact of each element on the performance. The table relates the elements to the physical and electrochemical aspects discussed in the previous section [5].

I_{PH}	Constant photocurrent source (electrons injected Dye→TiO_2)
Z_2	Impedance (D_2 and C_2) related to TiO_2/Dye/Electrolyte interface. D_2 diode like response, represents recombination processes.
R_{SH}	Resistance parallel to the photocurrent source, due to back electron transport in TiO2/Dye/Electrolyte interface.
R_3	Resistance correspondent to redox species diffusion.
Z_1	Impedance (R_1 and C_1) due to charge transfer at Pt electrode.
R_h	Resistance corresponding to TCO sheet resistance.

Table 2.3: Description of the equivalent circuit elements.

In a steady state, capacitances C_1 and C_2 can be neglected. Also, R_3, R_1 and R_h can be summed in one single series resistance. This way, the equivalent circuit becomes similar to a conventional solar cells equivalent circuit, known as 1 diode model [12][5], as seen on Figure 2.4.

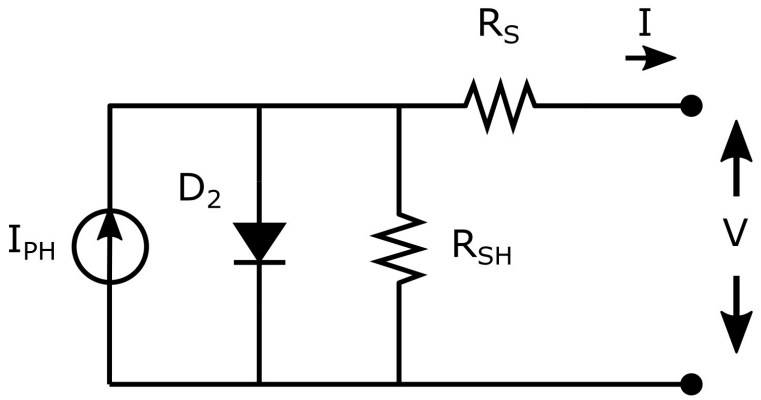

Figure 2.4: One diode model of a photovoltaic cell, including DSSCs.

From the 1 diode model, the relation of external current and voltage can be expressed as formula 2.3 [5].

$$I = I_{PH} - I_0 . \left(\exp\left(\frac{-q.(V - I R_S)}{m K_B T} \right) - 1 \right) + \frac{V - I R_S}{R_{SH}} \quad (2.3)$$

I_{PH} is the photogenerated current
I_0 is the dark saturation current
m is the ideality factor
R_S is the series resistance
R_{SH} is the shunt resistance
k_B is the Boltzmann's constant
q is the elementary charge
T is the absolute temperature

Equation 2.3 gives the current for each value of voltage, if kept temperature (T) and illumination intensity constant (which impacts I_{PH}) it is possible to obtain the so called IV curve of the solar cell, a very useful representation of the electrical behavior of the device [13]. Usually this is done under STC (standard test conditions) in which the cells are illuminated under 1000 W/m^2 (100 mW/cm^2) irradiance, a constant temperature of 25ºC and AM1.5G solar spectrum. This condition is often provided by a solar simulator, as will be discussed in section 5.2.10.1.

Since the current generated by a solar cell is directly proportional to its active area, it makes much more sense to analyze the current density, instead the absolute current generation. The current density is the absolute current divided by the active area, which is the

area of the cell containing absorbing material and actually participating in the power conversion.

The cell response is then represented by a JxV curve (current density versus voltage), as seen on Figure 2.5, which actually is one of the cells fabricated in this work and well aligned with the expected behavior from formula 2.3.

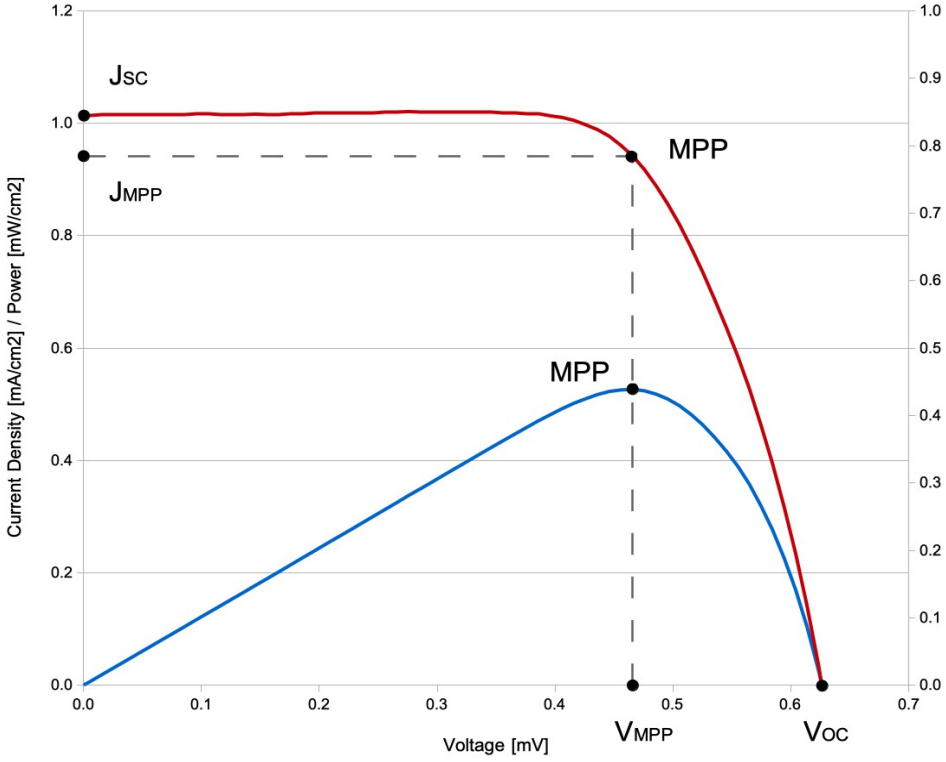

Figure 2.5: Typical JxV curve of a DSSC.
NDSSC made with dyes extracted from coffee leaves.

The following parameters are the most important on any solar cell characterization. Most of them can be observed on JxV curve (Figure 2.5) and easily understood. Fill factor (FF) and efficiency (η) must be calculated as will be described below [13].

V_{OC} (Open circuit voltage – voltage when in an open circuit condition)
J_{SC} (Short circuit current density – short circuit condition)
P_{MPP} (Maximum power point – maximum output power)
V_{MPP} (Voltage at maximum power point)
J_{MPP} (Current at maximum power point)
FF (Fill factor – see below)
η (Efficiency – see below)

Fill factor is another important parameter for solar cells characterization. It indicates the quality of the cell [5] and is closely related to series and shunt resistances. Increasing the shunt resistance and decreasing the series resistance will increase fill factor, because V_{MPP} and I_{MPP} will come closer to the theoretical maximum [5]. This parameter is calculated using the formula 2.4.

$$FF = \frac{V_{MPP} \times I_{MPP}}{V_{OC} \times I_{SC}} \tag{2.4}$$

Efficiency informs how much of the total light power incident on the cell active area is converted to useful electric power. Efficiency can be calculated using the formula 2.5.

$$\eta = \frac{P_{MPP}}{P_{SUN}} \tag{2.5}$$

η is the cells overall efficiency
P_{MPP} is the power generated at the maximum power point.
P_{SUN} is the power of the incident light.

Sun irradiance defined by STC (Standard Test Conditions) is 1000 W/m^2 or 100 mW/cm^2 [14] which is also the incident light power density (P_{SUN} / A). Thus, the above formulas can be arranged as in 2.6:

$$\eta = \frac{V_{OC} \times J_{SC} \times FF}{100} \quad \text{(STC)} \tag{2.6}$$

2.2. Photoanode

2.2.1. Substrate

As presented in the scheme of Figure 2.1, light must pass through a transparent anode, to reach the active layer formed by the semiconductor layer sensitized by the dye. Thus, plastic and glass substrates are often used. From the plastic side, transparent substrates made of PET (polyethylene terephthalate) are the most common options. For the purposes of the present work, glass substrates with a thin layer of TCO (transparent conductive oxide) were utilized.

The most common TCO options for glass substrates are: FTO (fluorine-doped tin oxide) and ITO (indium tin oxide). Qiao et al. [15] fabricated DSSCs with both options and compared their performances. The group found that FTO exhibits better results, which is in accordance with the regularity that this substrate is chosen by NDSSCs research groups.

2.2.2. Mesoporous TiO_2 nanoparticles film

As seen on section 2.1, DSSC photoanode is made of a mesoporous layer of semiconductor material which provides an enormous internal surface for the dye molecules to bond [7]. The preferable semiconductor material is titanium oxide (TiO_2) because of its high band gap, low cost, abundance, non-toxicity and higher cells efficiency than other materials, like ZnO or SnO_2 [4][6]. TiO_2 is commonly used as a paint base in pigment industry [5]. Also, its conduction band coincides well with the LUMO level of natural pigments (specially with anthocyanins) [4].

Cahen et al. [10] explain that the mesoporosity and nanocristallinity of the semiconductor are important not only to achieve a large surface area for dye adsorption, but also to allow the TiO_2 particles to become almost completely depleted upon immersion in electrolyte (considering the particles small size), and the proximity to all particles makes screening of injected electrons, and thus their transport, possible.

2.2.2.1 Thickness

The strategy to determine the most efficient mesoporous film thickness is behind a balance between light harvesting area and necessary diffusion length. If the thickness is increased, the internal surface area of the film will increase and much more dye-molecules can anchor to the surface, harvesting more light. At the same, electrons have a limited diffusion length, which depends on the TiO_2 particles diameter, porosity and neck size [5]. If the film is too thick, electrons will not be able to reach the substrate TCO and will be lost.

Many authors optimized the cells performance with TiO_2 layer thickness below 10 μm [16][17][18].

2.2.2.2 $TiCl_4$ treatment

The use of titanium tetrachloride to improve DSSC efficiency is becoming more often among researchers. Ghann et al. [17] consider it as one of the reasons for the enhanced efficiency achieved by their cells fabricated with pomegranate extracted dye. The explained reason by the authors is the creation of more sites for dye adsorption.

This treatment is usually done after TiO_2 annealing, dipping substrates in $TiCl_4$ solution for periods of time between 30 min to 1h, and then annealing them again [17][19]. Shirkavand et. at. [18] used $TiCl_4$ 40 mM aqueous solution at 70ºC for 30 min before and after TiO_2 sintering steps for the fabrication of DSSC using N719 synthetic dye and blackberry extract.

2.2.3. Dyes

The most often semiconductor oxide used in DSSC is TiO_2, a high band gap material, Thus, the light harvesting must be done by dye molecules attached to its surface. The ideal dye should absorb light in all visible wavelength range and has anchoring groups suitable for a firm attachment to the semiconductor oxide [20][4].

Due to the high efficiency and stability, ruthenium based dyes, such as N3, N719, N749 and black dyes has been used for TiO_2 sensitization since DSSC invention [7][6], despite the fact this component is one of the most expensive in DSSC [5]. Besides, these dyes exhibit other disadvantages: noble metal scarcity, toxic raw materials, and also sophisticated synthesis and purification steps [5]. For these reasons, natural dyes has been studied as a substitute of synthetic dyes.

Natural dyes are environmentally safe, fully biodegradable, non-toxic, easy to prepare, cost effective and widely available [6].

TiO_2 particles size often used range from 20 to 25 μm in diameter, while dye particles size ranges from 1 to 3 μm. For the efficient electron injection from the dye molecule to the nanostructure TiO_2, it is necessary a strong adsorption. This is achieved via anchoring groups, such as carboxyl, carbonyl and hydroxyl (Figure 2.6) located on the dye molecules [17]. Increasing the number of anchoring groups in the dye enhances sensitization and efficiency, this happens inherently in *Kigelia africana* due dye composition [21].

The better is the bond between dye molecules and TiO_2 surface, the better will be the electron injection and the cell overall performance [4].

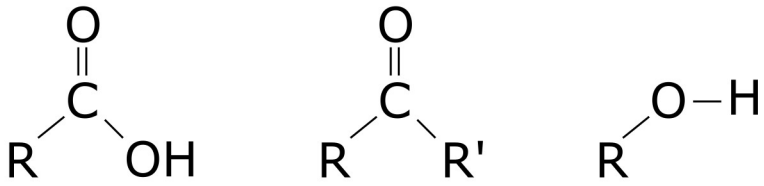

Figure 2.6: Dyes anchoring groups.
From left to right: carboxyl, carbonyl and hydroxyl.

In short, some important characteristics that the utilized dye must offer for a good cell performance are listed below [18][4].

- High light absorption in visible range
- Strong interfacial bond with semiconductor
- Easy electrons injection in TiO_2 layer (TiO_2 CB matching Dye LUMO)
- Quick reduction by redox pair (HOMO lower than redox potential)

Natural dyes can be used to replace the more expensive and toxic synthetic dyes, although efficiency and stability still need improvement for this alternative to be considered. Kumara et. al [4] points several advantages of natural dyes over synthetic ones:

- Simple preparation technique
- Low cost of production
- Complete biodegradation
- Easy access
- High availability
- Purity grade
- Environmental friendliness
- High reduction of noble metals usage

Section 3 offers a deeper look into natural dyes and their application in DSSC.

2.3. Electrolyte

Electrolyte is one of the key components of DSSC because it offers a path for the electrons to regenerate the oxidized dye molecules, as seen in equation IV of Table 2.1. This component is usually a low viscosity liquid so it can penetrate the porous of TiO_2 film and reach all adsorbed dye molecules [11]. However, extra care must be taken on DSSC sealing to avoid leakage and evaporation [6].

As seen in section 2.1, electrolyte working principle is based on a redox pair, usually I^-/I_3^-. When electrons come to the cathode, in the presence of a catalyst (usually Pt or C), they reduce I_3^- ions in the electrolyte to I^-, these ions rearrange themselves in the liquid so they can find the oxidized dye molecule attached to the surface of the semiconductor (TiO_2), reducing it and become again its oxidized form I_3^-.

Iqbal et al. [8] reviewed many studies on NDSSC and indicates several types of electrolytes been used, with different performances and characteristics, such as: LiI, KI, NaI and solid polymers.

Shalini et al. [6] explained that the risk of evaporation and leakage motivated the search for other options of electrolyte under development. One of the mentioned options is polymers consisted of metal salts of low lattice energy dissolved in polymer matrices such as ether, ester or amide, which show advantages such as thermal stability, high ionics conductivity and ease for cell assembly.

2.4. Cathode

2.4.1. Catalytic film

The presence of Pt or C (graphite) promotes and accelerates the reduction process of the iodine to iodite ion in electrolyte solution [22].

Platinum (Pt) is an excellent catalyst to I_3^- reduction and has a high back light-

reflection effect, but on the other hand, it is a rare and expensive material for large scale production. Besides, Pt corrodes with I_3^-, generating PtI_4 which impacts its durability. Thus, alternatives are been studied, such as: carbon nanotubes, graphite and conductive polymer. [4] [6].

Ghann et al. [17] used graphite and considered it as one of the reasons for improving performance.

Amadi et al. [23] used carbon soot as catalytic material, passing substrates over a candle light to cover it with a carbon layer.

2.5. DSSC Stability

Although ruthenium based synthetic dyes exhibit excellent efficiency and stability, DSSCs are subject to other degradation processes that may compromise the long term operation. Electrolyte is usually a low viscosity liquid, so it can penetrate the porous of the semiconductor layer to reach the dye molecules. Leakages and evaporation may disable the cell [6].

Corrosion of Pt caused by the reaction with I_3^- ions present in the electrolyte (in PtI_4 form) may also reduce conductivity and the cell overall efficiency [4].

NDSSCs are even further impacted, since they are fabricated by natural organic materials (e.g.: anthocyanin or chlorophyll). Free electrons on the surface of TiO_2 may react with moisture to produce free radicals which destroy organic molecules [21]. A deeper look at natural dyes degradation is provided in section 3.5.

Except for the reaction between Pt and I_3^- ions, the other above reasons bring an enormous importance for the cell sealing. Avoiding electrolyte leakage and moisture infiltration is imperative for a long lasting DSSC.

3. Natural Dyes

Singh et al. [24] affirm: “The use of green energy materials (natural dyes) in the fabrication of DSSCs has proved to be an alternative source of energy production as it does not contain rare, toxic and inorganic metal ions”.

Shalini et al. [6] also highlights the higher cost and toxicity of synthetic dyes, and add: “Natural sensitizers contain plant pigments such as anthocyanin, carotenoid, flavonoid, and chlorophyll that are responsible for chemical reactions such as absorption of light as well as injection of charges to the conduction band of TiO_2”.

Dyes containing useful pigments for DSSC fabrication can be easily extracted from natural products, such as: fruits, flowers, leaves, seeds and barks [6].

Despite of the many advantages of natural dyes, there are several reasons for a reduction on electron injection (Dye→TiO_2) and J_{SC} of the device, such as: low interaction with TiO_2 surface, distance between the dye skeleton and point of connection to TiO_2 surface, masking and agglomeration of pigments, which also reduces the absorption of light [4].

All this issues along with stability problems (discussed later in section 3.5) present the challenge, and also, an interesting opportunity for researchers.

Natural dyes usually have few main pigments. The most common molecular structures studied and applied to DSSC fabrication are: betalains, carotenoids, flavonoids (i.e. anthocyanins) and chlorophylls [16][19][24][4]. The present work concentrated the study of DSSC using anthocyanins and chlorophylls as sensitizing dyes.

3.1. Anthocyanins

Flavonoids are the main pigment associated to the colors of flowers in angiosperms plants. They are present in chromophores and are responsible to attract insects and protect the plant from UV-B light [4]. Flavonoids require less energy for a HOMO to LUMO transition and are rapidly adsorbed to TiO_2 surface [6].

Among all flavonoids, anthocyanins are one of the largest and most important group. Accumulated in cells vacuoles, anthocyanins color varies depending on the pH (red, purple or blue). In leaves they have the function of protection, screening the excess light from the Sun, specially in the UV and blue-green ranges. In flowers anthocyanins attract pollinator due their vibrant colors [20].

Anthocyanins are glycoside with anthocyanidin (flavonoid) C_6-C_3-C_6 skeleton (figure 3.1). The most common are pelagonidin (orange), cyanidin (orange-red) delpinidin (blue-red), peonidin (purplish-red), petunidin (blue-red) and malvidin (blue-red) [18].

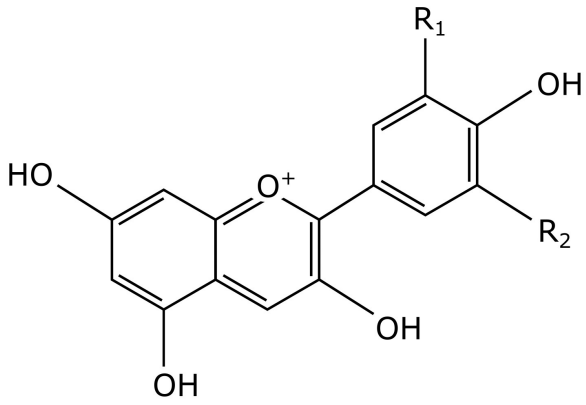

Anthocyanidin	R_1	R_2
Pelagonidin	H	H
Cyanidin	OH	H
Delpinidin	OH	OH
Peonidin	OCH_3	H
Petunidin	OCH_3	OH
Malvidin	OCH_3	OCH_3

Figure 3.1: Molecular structure of common anthocyanidins.

Besides the high absorption coefficient in visible range, anthocyanins are adsorbed to TiO_2 particles surface by strong anchoring groups: hydroxyl and carbonyl. This mechanism facilitates the electron injection between the dye and the semiconductor [17][4].

Iqbal et al. [8] concluded from results collected from several references that anthocyanins better injects electrons than other pigments, better adhere to TiO_2 surface, and dyes containing anthocyanin are more efficient comparing to other natural pigments. Shalini et al. [6] also confirms the better results from anthocyanin in comparison with other pigments.

3.2. Chlorophylls

Chlorophyll is the pigment which gives the plants the green color. It is responsible to harvest the energy light in the leaves as part of the photosynthesis process. This is mainly achieved by its spectral properties. The main types of chlorophyll are: chlorophyll “a” and chlorophyll “b”, the last has a more blueish spectrum with a redshift [6]. Figure 3.2 shows the molecular structure of chlorophyll “a” and chlorophyll “b”.

As anthocyanins, chlorophylls are being largely used in DSSC research. Many plants, specially leaves extracts, have been tested as sources of chlorophylls. Overall efficiencies have already overcome 1% in several published works [4][6].

Chlorophyll have also been modified for better adsorption on TiO_2 surface, and thus, improved efficiency. Kay and Grätzel in 1993 demonstrated the use of copper chlorophyllin to achieve 2.6% overall efficiency under simulated sunlight illumination [25].

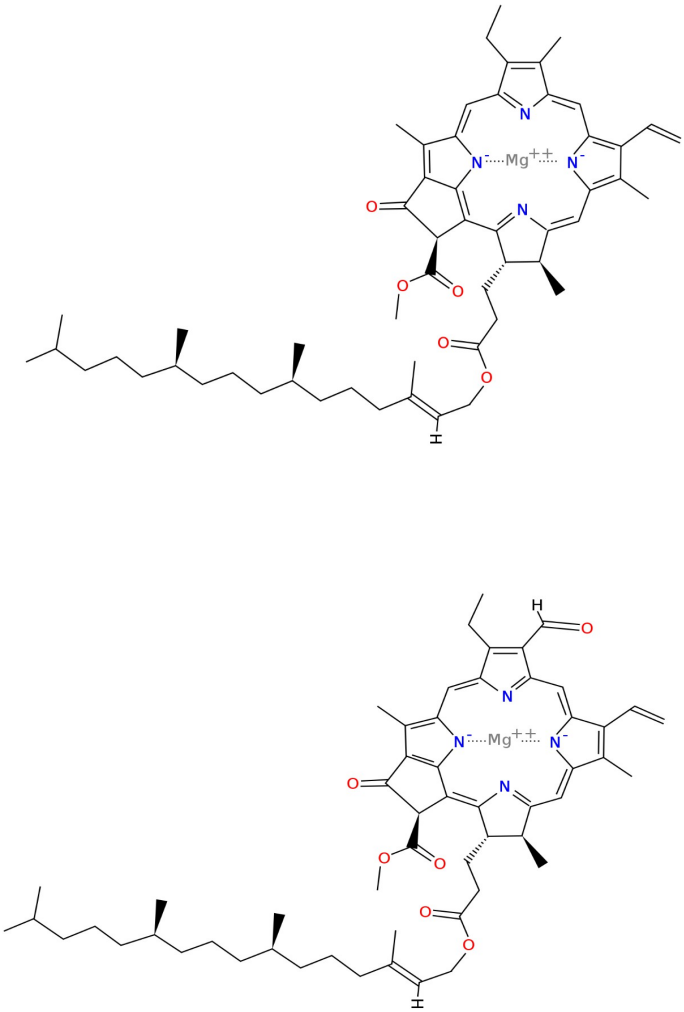

Figure 3.2: Molecular structure of chlorophyll “a” (upper figure) and chlorophyll “b” (lower figure).

3.3. Dye preparation

Basically natural dye preparation for NDSSC fabrication requires 2 basic steps:

1. Plant processing to obtain an extract, which may involve the dissolution in a solvent (usually water and/or alcohol).
2. Extract filtration and purification. Usually paper filtering and centrifugation, but may include others like chromatography and lyophilization.

There are many reported protocols for both steps in the available literature. Some are simple, others require special equipments and more time-consuming techniques.

3.3.1. Plant processing

Jasim et al. [26], used a drying step at ambient temperature to transform Curcumin

extract in a glass like residue for dissolution in methanol. Leyer et al. [27] also dried, ground and sieved maqui berry and blackberry fruits for later dissolution in water. This technique completely eliminates the water from the plant or the acetonitrile used for extraction, but must be held in low temperature to avoid dye degeneration.

de Silva et al. [16] did not use drying step during plant processing but included chromatography for purification of carotenoid and anthocyanin extracted from mondo-grass berries and blackberries. They also kept the extract and pulp in the refrigerator for 24h for saturation.

3.3.2. Extract purification

Ghann et al. [17] consider dye purification, among others, a reason for the enhanced efficiency achieved by their pomegranate based cells. Amadi et al. [23] also emphasize the homogeneity and rigorous purification through filtration and centrifugation.

On the other hand, Singh et al. [24] obtained 1.76% efficient cells using the extract of *Begonia malabarica* without further purification, just refrigerated centrifuge (10 min at 1500-3000 RPM).

After dye purification, storing can be done in low temperature (e.g.: 5ºC [27]) avoiding light exposure [27][24].

3.3.3. Solvent

Several solvents can be used during dye extraction from plants, the most commons are water, ethanol, methanol and organic acids. Iqbal et al. [8] states that the chosen solvent will impact on the dye adsorption and the cell performance. Also, ethanol and water yield better results.

Kumara et al. [4] also highlights the importance of solvents during dye extraction, adding: “reported results showed that the performance does depend on the solvent properties such as polarity, acidity, dye combination and temperature”. They also state that the anchoring behavior is dependent on the solvent and dye extracted, which will affect the cell overall performance.

Singh et al. [28] affirm: “Although there are many factors which determine absorption of light by dyes thereby affecting efficiency of DSSCs immensely, an important role is also played by the dye extracting medium, i.e. solvents. For an extraction to be efficient the polarity of the extraction solvent should match the compound and also the solvent must be able to dissolve completely the target compound(s)”. In the same work, the group compared water and ethanol as solvents for extraction of *Melastoma malabathricum* L. dye. For the conditions of their experiment and the chosen plant, it was found water as a better solvent, cells exhibited more efficiency and stability due to better solubility of the dye in water and functional groups properly attached.

But it appears that a good solvent for one plant, may not be the best option for another. The same group, Sigh et al. [28] which found water as better than ethanol for *Melastoma malabathricum* L. had excellent results (efficiency of 1.76%), 3 years later, from *Begonia malabarica* L., but this time using ethanol instead [24].

Calogero et al. [22][19] reported better sensitizing activities, better charge injection and much more stable solar cells by adding organic weak acids such as: acetic acid, malic acid, tartaric acid and citric acid, to the extract until pH = 2.0 is achieved. Inorganic acid such as HCl was also used to further lower the pH to 1.0. Organic acids were also used by other authors. Shalini et al. [21] used citric acid for the dye extraction from *Kigelia africana* flower. The group reported improved sensitization and better stability properties than other solvents. Kumara et al. [4] explain that the use of acid by some groups has improved cell performance by inhibiting aggregation of dye molecules and facilitating electron injection.

Sometimes, depending on the species being used for dye extraction, solvent is not necessary. Singh et al. [24] did not add any solvent for the extraction of *Punica granatum* since the fruit seeds contain water.

3.4. Dye adsorption

3.4.1. Sensitizing time

Jasim et al. [26] used a 24 hours anode soaking time for TiO_2 dye adsorption. Leyer et al. [27] concluded in their work that an impregnation time of 8h yields better cells than 24h for maqui berry and blackberry fruits.

Colagero et al. [22] consider that the sensitizing or dipping time should not exceed 2 hours at 20ºC to 25ºC for DSSC fabricated using a mix of dyes extracted from a red radicchio and Sicily blood oranges.

3.5. Natural dye stability

DSSCs are already subject to stability problems due to leakage of liquid electrolyte and Pt catalyst degradation [5], as discussed in section 2.5. Additionally, in NDSSC there is the dye degeneration also impacting the cell long term stability.

Shalini et al. [21] explain a dye degeneration process in NDSSCs: "TiO_2 is commonly used as photo electrode for DSSC. They exhibit good characteristics necessary for a photo electrode but their photo catalytic activity in presence of sunlight produces free electrons on the surface. These free electrons on reaction with moisture produce free radicals, which destroy the nearby organic matter".

On the study of the natural dyes photo-degeneration, Tennakone et al. [29] made a clever and elucidating experiment. Cells were made using a mesoporous layer of TiO_2 sensitized with cyanidin from Anthurium flowers, but in an open assembling, so the photoanode could be exposed to the environment atmosphere (CuI was used as electrolyte and

gold-plate TCO/glass as back contact). The cells were placed in a illuminated thermostable chamber where the light and atmospheric conditions could be controlled. The group could test the cells performances over the time, under moist air, dry air, dry argon (oxygen free) and moist argon. Besides, illumination was provided from different sources with and without UV light. With the experiment, the group could isolate each factor impacting the dye degeneration, and their contribution:

1. Direct **UV light** dye degeneration due to molecule bonds breaking by high-energy photons absorbed by the dye.
2. Electrons on the TiO_2 surface reacts with **oxygen** (if present) creating the superoxide ion (O_2^-) which reacts with oxidized dyes (Dye^+).
3. **Moisture** enhances the photo-decomposition of the dye molecule. Holes generated by TiO_2 excitation by high-energy photons are scavenged by hydroxyl ions to form highly oxidative OH^O free radicals that rapidly attack the dye.

Thus, the authors highlighted the importance of a fabrication process that can avoid inclusion of moisture and oxygen, and the selection of a pigment that does not absorb light in the UV region of the spectrum.

4. Maximizing efficiency

Like other PV technologies, DSSC are evaluated by its capacity to reduce the LCOE (levelized cost of energy) which is given by the concept of triangle (efficiency, stability and cost). The three are very important, however due to comparisons with more mature silicon technology, efficiency is been given special attention [5].

Furthermore, natural dye-sensitized solar cells (NDSSC) offer important advantages over their already commercially available synthetic dye version. This low cost and environmentally safe option has been studied by many researchers around the globe, searching for ways to improve the factors still prohibiting commercial availability, i.e.: stability and efficiency.

This work brings relevant information on stability on section 3.5, but the focus is the efficiency improvement aspects. In this section, it will be presented some insights and study on this regard.

Kumara et al. [4] offered an excellent literature review on the use of natural dyes in DSSC. Their work highlights some important aspects to be considered, such as the factors researchers can adjust to maximize the function of dyes:

- Dye concentration
- pH
- Extraction techniques
- Co-pigmentation from other sources
- Sensitization methods
- TiO_2 nano particle size
- TiO_2 film thickness
- Sensitizing/soaking time
- Electrolyte composition

The above are some variables researchers may use to improve their processes and maximize NDSSC performance. In the present work, most of them were experimented, or at least taken into consideration during processes design and materials selection.

Researchers must find ways to improve light harvesting and reduce losses. On section 2.1 the main loss mechanisms were discussed. Besides recombination factors, Ardakani and Arazi [30] explain other unwanted processes that lead to losses in V_{OC} and J_{SC}. Strong intermolecular interaction between dye and TiO_2 causes decline of J_{SC} due to dye molecules aggregation, which reduces TiO_2 surface area available for other molecules and facilitates dye relaxation and recombination with electrons on TiO_2 surface. Also, TiO_2 protonation (collection of a proton due to surface electric potential) changes the amount of dye adsorbed and decreases stability. The authors could reduce these loss mechanisms by the addition of a co-adsorbent, its function was to compete with dye molecules for the TiO_2 surface adsorption, reducing dye aggregation and protonation, thus improving charge injection and electrons

lifetime.

Cahen et al. [10] presented that an obvious cause for low fill factor is the recombination of TiO_2 electrons with triiodide in the electrolyte in an increased rate as the TiO_2 becomes more negative, which also reduces photocurrent. This is connected with the increased efficiency achieved by Ardaki and Arazi [30], above.

The authors also explain that differences in V_{OC} obtained from different dyes are mainly caused by recombination rates. This can also be observed in the equivalent circuit (Figure 2.3), the diode D2 represents well the recombination processes, which increases with the device voltage.

5. Fabrication

The structure used for the present work elaboration was developed from scratch, including the laboratory itself. This author started with the passion for the subject, a limited budget and some available space.

Established to serve as a photovoltaic research and education facility, the new laboratory was a house purchased by Max School, an elementary and middle school located in São Paulo, Brazil, as part of its expansion. The laboratory space was remodeled to give room for the necessary equipments and furniture.

Important difficulties arose from the lack of an initial infrastructure, but the biggest challenge was to develop the fabrication protocol. Most similar research works could count on a well-established team, infrastructure, and exhaustively tested and optimized protocols. Although some research teams have shared the most important steps of their protocols through many publications, it was necessary to review and adjust each step to better fit the conditions and goals of this new laboratory.

Thus, most of the time of this research effort was focused on learning and adapting techniques described on the literature to design and optimize a fabrication protocol.

5.1. Laboratory construction

One of the advantages of DSSC technology is the use of low to medium-purity materials [7], this is even more noticeable in NDSSC. As stated by Gong et al. [5], "DSSC are easy to fabricate since they are insensitive to environment contaminants and processable at ambient temperature".

Considering the above, a clean room could be avoided. However, even utilizing a simple infrastructure, attention to several factors were taken during laboratory design and construction, such as:

- Temperature and humidity control
- Clean space, free from outside direct ventilation
- Clean surfaces and closed storage units
- Use of de-ionized water for cleaning and solutions preparation
- Fume hood with adequate exhaustion system

Too many details on the laboratory design and construction will be skipped in this work, however a few main points will be discussed below for those who may find themselves in a similar challenge.

After planning the necessary infrastructure and the space organization, the upper floor of the acquired house was completely demolished and the space (about 35 m^2) open for the utilities installation (electric connection, illumination, plumbing and exhaustion system). Then

an easy cleaning floor, without joints which could accumulate dirt was installed. Later, the furniture and equipments were installed. Laboratory pictures during and after construction can be seen on Figure 5.1.

For DSSC study, a few working areas were created:

- Wet area (cleaning substrates and glassware, solutions preparation, etc)
- Dry workbench (substrates preparation, films deposition, assembling, etc)
- Characterization workbench (Optic and electric measurements after fabrication)
- Electronic workbench (Equipments maintenance, boards assembling, etc)
- Office area (computer area, study)
- Meeting area (5 to 6 people for education)
- Several storage units (components, chemicals, glassware, materials, etc)

Figure 5.1: Laboratory pictures during and after construction.

Despite of the climate control done by an air conditioner system, the laboratory was not air sealed and external humidity could penetrate. It was noticed that in rainy days, the cells tended to be less efficient, certainly due to humidity penetration in the films, specially the TiO_2 layer. Thus, during the whole fabrication process, the laboratory humidity sensor were monitored and AC adjusted accordingly.

5.2. Fabrication protocol

After the laboratory construction and the main equipments purchased or made (more details ahead), it became time to start fabricating cells and develop a protocol.

The strategy was to start the fabrication using a basic protocol developed from a reliable source. The document “Dye Solar Cells for Real” [31] published by the Swiss company specialized in solar cells supplies Solaronix, proved to be an excellent start. The simplicity and detailed description of procedures were a highly valuable starting point.

As suggested by the document, blackberry (*Rubus* spp.) were chosen as dye source during all the present work, for the study and maximization of all other NDSSC aspects besides the dye. This choice was also aligned with one of the goals of this work, the use of Brazilian plants, since blackberry is also a naturally found plant in Brazil, known in Portuguese as “amora-preta”. Figure 5.2 shows a picture of a box of blackberries as purchased from a local market.

Figure 5.2: Blackberries as purchased from a local market.

It was decided to study all relevant references and apply improvements to the protocol for each fabricated batch, optimizing the blackberry dye cells as much as possible before testing other plants. This way, it was possible to compare different plants in the end of the work, with the cells fabrication protocol already improved.

Each fabricated batch had specific goals, such as: testing a sealing technique, determine the best TiO_2 layer thickness, sintering temperature, etc. The batches were numbered by the fabrication date (YYYYMMDD) for easy reference and access to data.

In this section the batches fabricated for protocol optimization will only be briefly

described to avoid repetition of the same methods and materials, since one or two parameters are varied (those will be detailed). However, in the end of this section the whole defined protocol is presented in details.

5.2.1. Performance references

One of the first steps taken for the protocol development was the study of methods and reported results by other authors, specially the ones which also used blackberry fruit for dye extraction. Thus, it was possible to almost directly compare parameters, such as V_{OC}, J_{SC}, FF and η.

The main fabrication parameters used by those authors are listed in Table 5.1. The achieved results reported in the same publications can be found in Table 5.2.

Ref.	TCO	Clean.	$TiCl_4$	TiO_2 thick.	Sintering	Cathode	Solvent and Extraction	Sensitizing	Electrolyte
[16]	FTO	KWNWI	No	1.5µm	450ºC/20'	Pt	Methanol (Vacuum filtration)	N.I.	I^-/I_3^-
[32]	N.I.	N.I.	N.I.	N.I.	N.I.	Graphite	Water/Ethylene Glycol (Paper filtration)	N.I.	KI/I
[20]	N.I.	N.I.	No	N.I.	N.I.	N.I.	Water (Filtration/Centrifug.)	N.I.	N.I.
[17]	FTO	N.I.	Yes	7µm	380ºC/2h	Graphite	Water (Centrifug/Lyophiliz.)	50'	I^-/I_3^-
[22]	FTO	N.I.	No	10-20µm	450ºC/30'	Pt or C	Water/Acids (Paper filtration)	2h	I^-/I_3^-
[19]	FTO	DWE	Yes	9.3µm	500ºC/30'	Pt	Acids (Filtration)	2-8h	Several
[33]	FTO	N.I.	Yes	7-10µm	450ºC/30'	Pt	Methanol/Acids/Water (Filtr./Chromatog.)	N.I.	KI/others
[18]	FTO	DWE	Yes	2µm	2x 500ºC/30'	Pt	N.I.	N.I.	I^-/I_3^-

Table 5.1: Fabrication parameters of literature references using blackberry for dye extraction.

Column “cleaning” in the Table 5.1 refers to the utilized techniques for substrates cleaning (K = KOH, W = DI Water, N = HNO_3, I = Isopropanol, D = Detergent, E = Ethanol).

$TiCl_4$ column refers to the treatment presented in section 2.2.2.2, which was not used in this work due to difficulties found for this substance purchase. This fact must be taken in consideration when comparison between performances is made. Several authors emphasize the improvement on performance achieved by the use of this treatment, as discussed in section 2.2.2.2. Extraction column indicates methods and solvents used for dye extraction.

Ref.	V_{OC} (mV)	J_{SC} (mA/cm^2)	FF	η
[16]	557	0.475	67%	0.18%
[32]	720	7.100	51%	N.I.
[20]	500	0.700	50%	0.20%
[17]	460	11.160	26%	1.40%
[22]	400	1.570	66%	0.42% (water) 0.89% (acids)
[19]	320	9.000	57%	1.07%
[33]	400	2.100	N.I.	0.56%
[18]	770	8.320	70%	1.13%

Table 5.2: Performance parameters of literature references using blackberry for dye extraction.

It is interesting to notice in Table 5.2 how reported performances vary. All parameters exhibit a high variance, including efficiency. Besides the differentiation by specific characteristics of each work, the technology of using natural dyes for DSSC fabrication is still in an early stage, much still need to be done, tested and improved.

Although the above references were more frequently consulted (due to the use of blackberries), many other publications were studied and considered, most of those used other plants, but exhibited close similarities of the utilized fabrication processes. In special, three NDSSC literature reviews were very useful, they were [8][4][6]. All of them analyze in detail the achievements of many other important publications.

5.2.2. Improvement opportunities

One of the first batches fabricated (20191204) had the intention of only test the assembling techniques. The electrical parameters would not taken into consideration since concerns about materials preparation, parts alignment, assembly steps, etc were more relevant at that point. Thus, just by curiosity and casual observation, several solvents were used to extract the dye from blackberry fruits: ethanol, water, vinegar and lemon juice, with different concentrations, as seen in Table 5.3.

Even though it was not the goal for this batch, the electrical parameters were still measured (Table 5.4).

Cell	Fruit weight	Solvent type	Solvent volume
1	65 g	Ethanol	75 ml
2	65 g	Water	75 ml
3	65 g	Vinegar	125 ml
4	65 g	Lemon	125 ml

Table 5.3: Solvents and volumes used in batch nº. 20191204 .

Cell	V_{OC} (mV)	J_{SC} (mA/cm^2)	FF	η
1	522	0.308	50.38%	0.08%
2	472	0.349	55.26%	0.09%
3	502	0.278	57.84%	0.08%
4	482	0.309	55.96%	0.08%

Table 5.4: Cells parameters of batch nº. 20191204

The interesting fact was that even though the batch was focused only on assembling aspects, the found results for V_{OC} and FF were in an acceptable range if compared with the references (section 5.2.1). Efficiency was very low for all cells, and the cause was the low current.

These unexpected results were an encouraging fact to start the analysis of the parameters on the intention of finding ways to improve the fabrication protocol to reach better efficiency, specially by, although not limited to, the current increase.

All the physical and electrochemical aspects already detailed in section 2.1 were considered in the analysis, however special attention was dedicated to relate the electrical parameters found in batch 20191204 to the DSSC equivalent circuit (discussed in section 2.1.1).

The first conclusion was that R_S (series resistance) and R_{SH} (shunt resistance) should be improved because FF was low (~50-56%), but they were not the most important reason for the very low efficiency. It should be another parameter with an even higher impact on the cells performance.

Attention then passed to the recombination processes, represented by the diode on the

equivalent circuit. If this diode was draining too much current, the impact would be high on FF, V_{OC} and J_{SC} simultaneously [4][30][10]. However, since the open circuit voltage (V_{OC}) was in acceptable range (comparing with references in section 5.2.1) it still should be something else impacting the performance at that level.

Thus, by exclusion, the photocurrent source must be the main problem for the so low performance. The cell was losing efficiency from several reasons, of course, but the photocurrent was certainly the weaker aspect.

With that conclusion, although all other opportunities for improvements would be considered, the main efforts would be dedicated to photocurrent increase, specially the factors presented by Kumara et al. [4] and discussed in section 4. The fabrication protocol was then studied and changed on the later batches having all that in mind.

5.2.3. Fabrication steps

The cells batches fabricated in this work were divided in two groups. The first (section 5) had protocol changes in every batch to maximize the fabrication parameters. This group was fabricated with 4 to 6 cells per batch, which was enough for parameters testing, but also, to keep time consumed and costs with materials down. The second group (section 6) used the protocol already maximized with the first group, with all parameters kept constant, except the change of the dye solution. Each batch in this group had 3 cells, since the goal was to compare batches by the performance of different plants as dye sources.

Basically, even with some variations, each cells batch was fabricated following the steps below:

1. Substrates preparation (holes drilling, scrape edges and cleaning)
2. Films deposition (TiO_2 on anode and Pt on cathode)
3. Anodes sensitization (adsorption of dye by TiO_2 film)
4. Electrodes joining (Parafilm® used as sealant and adhesive)
5. Electrolyte injection (through the cathode holes)
6. Holes sealing (Parafilm® and coverslips)
7. Metal contacts (attachment)
8. Characterization (V_{OC}, J_{SC}, FF, η, abs. spectrum, etc)

After taking the above steps, each cell had the structure presented on Figure 5.3, which also shows a picture of one of the fabricated cells.

The yellow area represents the liquid electrolyte and separates the photoanode (upper part) from the cathode (lower part). Both has TCO (transparent conductive oxide) depositions and metal contacts attachment. The cathode has also two holes, one for the electrolyte injection during assembly and the other for air escaping during injection. Parafilm® was used as sealant and adhesive to keep everything tightly together and avoid electrolyte leakage. The holes are also sealed with Parafilm® and a coverslip.

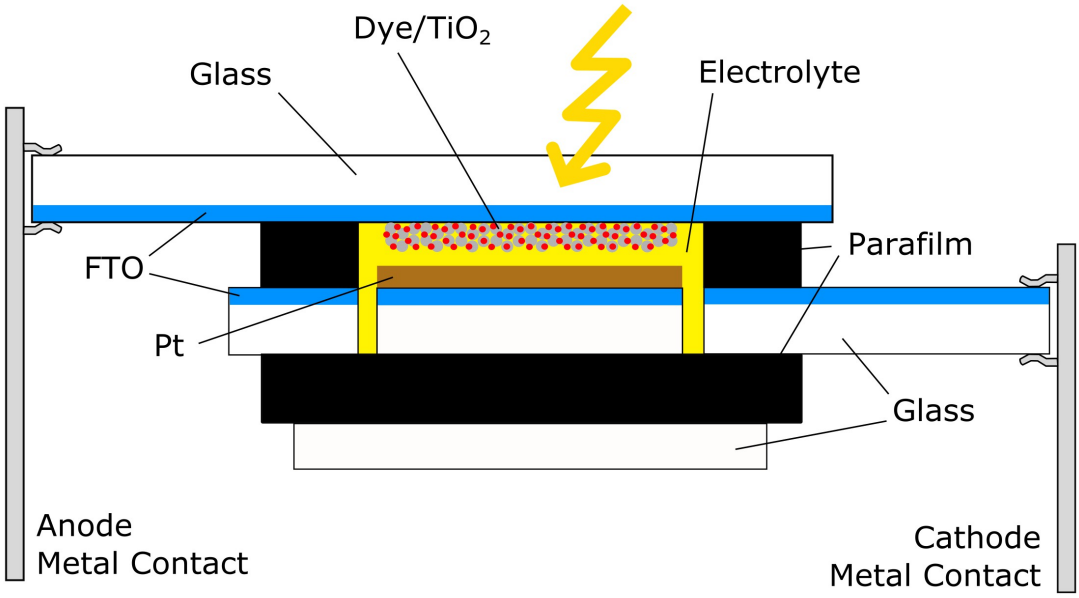

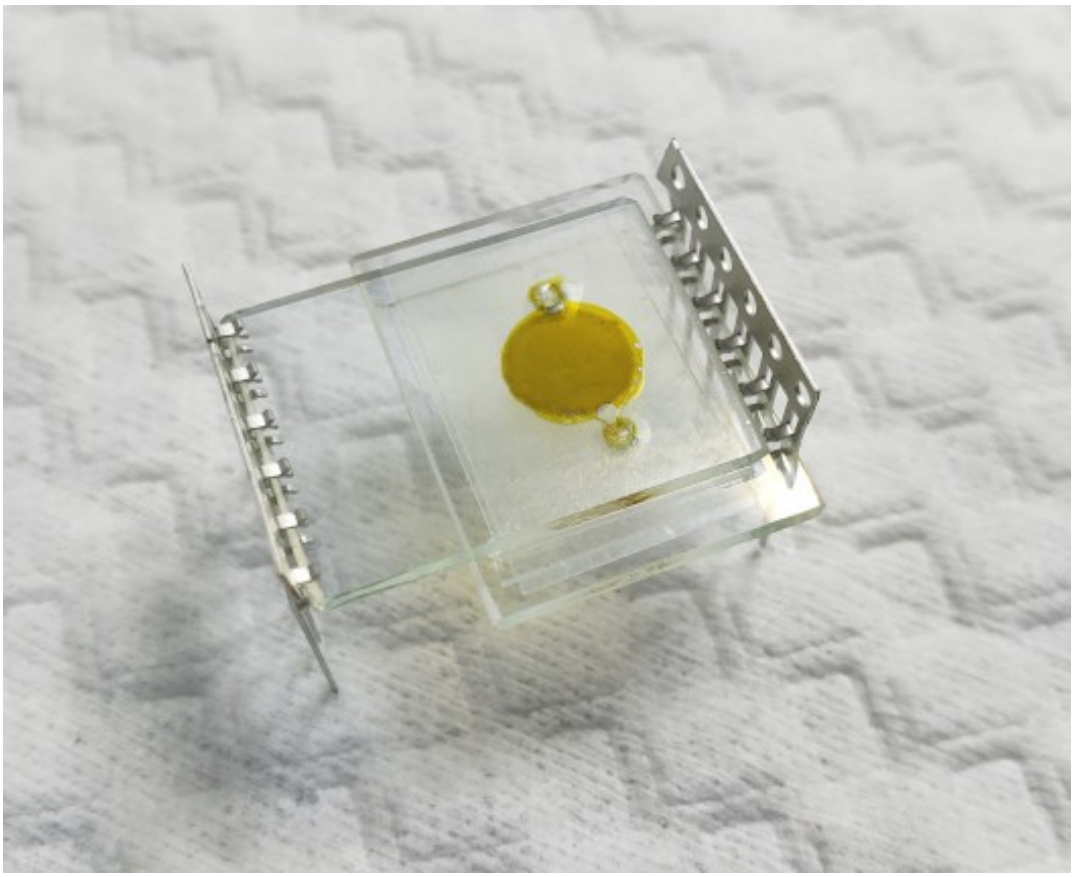

Figure 5.3: Scheme and picture of NDSSC fabricated.

A concern arose during fabrication scheme definition was the possible increase of recombination on the interface between electrons on anode TCO surface and electrolyte ions, specially in the space left between the TiO_2 area and the Parafilm®. Cahen et al. [10]

explained this recombination is unlikely because of the absence of the catalytic material. This information could be confirmed disassembling a cell and reassembling it with different areas left open. It was not possible to detect significant changes on the performance.

The most important aspects of the above fabrication steps will be discussed in details on the following sections.

5.2.4. Substrates preparation

The type of substrate selection were discussed in section 2.2.1. For the NDSSCs fabrication, two types of substrates were used: ITO and FTO glass substrates. Fabricated batch nº. 20200129 (Table 5.5) was used to compare both options and find which one would provide the best performance. Each substrate type was used for both electrodes (anode and cathode) and all other fabrication parameters were kept constant.

Due to the metal contacts selection (see section 5.2.9) and other assembling factors, it was necessary to use 1.1 mm thick glass, supplied by Ossila. The ITO and FTO substrates characteristics can be seen on Table 5.5, along with the performances of the best cells fabricated with each option.

Substrate	**Sheet resistance**	**Best cells performance**			
		V_{OC} [mV]	**J_{SC} [mA/cm²]**	**FF**	**η**
Ossila ITO S111 20 mm x 15 mm	14–16 Ω/□	534	0.427	65.40%	0.15%
Ossila FTO S302 20 mm x 15 mm	9.39 Ω/□	562	0.492	74.40%	0.21%

Table 5.5: Substrates used in batch 20200129 and best cells performance of each option. Sheet resistance measured by the manufacturer.

It can be noticed the 40% higher efficiency achieved with FTO substrates, in accordance with other publication findings [15]. The use of FTO yielded higher current and open circuit voltage. However, it also must be considered the contribution of the lower sheet resistance of the FTO substrate to fill factor, which of course, improves the efficiency.

After the fabrication of batch 20200129, it was decided to use FTO covered glass substrates in the next batches.

Protocol definition → FTO glass substrates (anode and cathode)

The first practical step for cells fabrication is the substrates preparation. For later electrolyte injection in the cells, two holes were drilled using a 2 mm diamond tip (designed for glass drilling). The holes were spaced approximately by the diameter of the active area, so electrolyte could be injected in one hole while air escaped by the other, until the volume were filled, avoiding bubbles as much as possible.

Then, in order to facilitate the attachment of the metal contacts to the electrodes, the glass substrates edges had to be sanded using a soft sand paper (220 grit). This procedure was done passing each substrate edge, of both sides, on the sand paper in 45º angle a few times (around 10), taking care to avoid to scratch the substrate surfaces, specially the conductive side. Figure 5.4 shows pictures of substrate preparation.

In the present work the used cleaning process followed references [19] and [18], with the addition of an acetone step. Successive periods in ultrasonic bath at 40ºC was taken as described below:

1. 50% alkaline detergent solution for 20-30 min
2. Wash with DI water 4 or 5 times
3. Acetone for 10 min
4. Ethanol for 10 min
5. Wait few minutes for drying

Figure 5.4: Substrate preparation and cleaning.

5.2.5. Films deposition

There are several ways to deposit TiO_2 and Pt layers. In this work, spin coating, doctor blade and screen printing were tried.

Spin coating was tried using Ossila® microcontrolled spin coater. Besides the good film quality and the ease to make virtually any thickness film just setting the proper rotation speed and time, for the intended goals, this method was too time consuming, since it is necessary to spin each substrate separately and clean the edges.

Doctor blade was used for several initial batches fabrication, it worked satisfactorily until thinners films were needed, for those, the irregularities on the film surface were visible. Also, the thickness is limited by the stencil being used.

The best quality was achieved, specially for very thin depositions, by the use of screen printing technique. Layers were better defined, smoother and the thickness could be well controlled by the mesh selection from an enormous variety of options.

The selection started consulting TiO_2 paste technical information [34]. The document suggested a 61–64 mesh (61 threads/cm and 64 μm thread diameter) which would provide a 4 μm TiO_2 layer thickness. In the same way, the Pt paste technical information [35] suggested a 68–55 mesh.

Thus, consulting the meshes catalog from a national manufacturer (Tegape® [36]) it was found options close to the suggested meshes. It was decided to purchase monofilament polyester meshes (appropriate for this application) from HD (high definition) line.

Furthermore, to optimize the film thickness it was necessary to test a variety of meshes, although close to the suggested ones. Having those points in mind, the catalog was transferred to a spreadsheet and the meshes open areas were multiplied by the meshes thicknesses, giving an arbitrary reference of the volume of paste that would be deposited by each mesh. From the results, mesh options were selected from the spreadsheet in a regular interval of arbitrary units of deposition material volume (~1000 a.u. interval), some above the suggested mesh by the paste manufacturer, and some bellow. This method offered a reference for the mesh selection, since the meshes characteristics vary in such a way that makes the decision very difficult. Table 5.6 shows the selected meshes characteristics, taken from the manufacturer catalog.

Mesh [threads/cm]	Thread diam. [μm]	Open surface [%]	Thickness [μm]	Thickness x open surf. [a.u.]
51HD	77	34	150	5100
61HD	70	31	140	4340
77HD	63	26	120	3120
140HD	38	23	80	1840

Table 5.6: Selected meshes from Tegape® catalog [36]. The last column gives a reference of deposition volume per area (arbitrary unit).

After the meshes selected, a template to place the substrates were fabricated, which aligned with a screen pattern, created on a computer vector design software. The screens were fabricated by a local company.

The screen pattern consisted of 2 rows of 4 circles for the TiO_2 paste printing (active area) for up to 8 anodes, and the same for the cathodes (8 circles for Pt paste printing). The circles on the screen were well aligned with the position of the substrates on the template. TiO_2 circles were 6 mm in diameter (active area = 0.2827 cm^2) while the Pt circles were 8 mm in diameter (0.5027 cm^2). Figure 5.5 shows a picture of the template and screens.

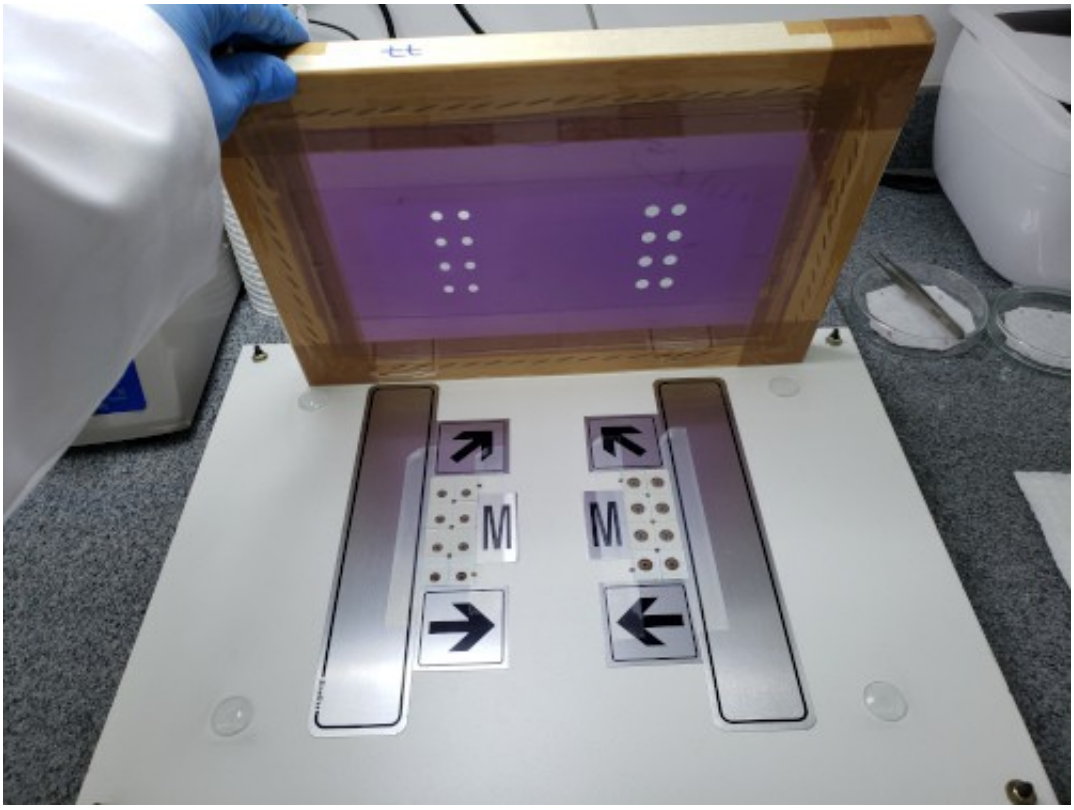

Figure 5.5: Pictures of the screen printing template and screens.
Meshes were tested for both anode and cathode.

The same meshes were also used for Pt paste printing on cathode. The pattern designed for the screens consisted of anodes and cathodes areas to be printed with the respective paste. Thus, placing the substrates on the template was possible to print either the anode or the cathode, just switching the screens and pastes.

A practical and interesting hint to be shared is the screens cleaning. Some screens meshes have very small open areas, if paste dried in those spots they became hard to remove, even with the same solvents used in the paste. If that happened, the next print exhibited flaws. So, it is a good practice to clean the screens right away with the appropriate solvent for the paste used. Also, the emulsion used for the screen development must be resistant to the same solvents present in the paste and used for cleaning. For this work, these concerns were discussed with the screens supplier before the order was placed.

5.2.5.1 Semiconductor film deposition (TiO_2)

As explained above, screen printing technique was used for TiO_2 layer deposition. The paste Ti-nanoxide T/SP [34] from Solaronix was used to print directly on the substrates surfaces. Batch 20200219 was used to find the best mesh for TiO_2 layer printing, 3 meshes were tested for this batch, which were enough to find the optimum option. The best cells obtained from this batch showed the results listed in Table 5.7.

Mesh	**V_{OC} [mV]**	**J_{SC} [mA/cm^2]**	**FF**	**η**
61HD	562	0.451	74.83%	0.19%
77HD	563	0.571	73.00%	0.23%
140HD	574	0.302	73.02%	0.13%

Table 5.7: Best cells from batch 20200219 used for comparison between meshes for TiO_2 film printing

The general cells quality were good, which can be observed by the FF above 73%. Current from 77HD is much higher. This is a very strong indication that the layer had adequate thickness, which also impacted the cell efficiency.

After utilizing the method described in section 5.2.10.5 (thickness measurement), the optimized TiO_2 film thickness (above) was measured in batch 20200303, made specially to confirm some procedures. The thickness found were: **2.83 ± 0.13 µm**. This thickness is in the range of other publications, as seen in section 5.2.1.

Protocol definition → Screen printing Tegape® 77-63 HD mesh for TiO_2 layer deposition (77 threads/cm and 63 thread diameter)

5.2.5.2 Catalytic film deposition (Pt)

As discussed in section 2.4.1, the most used catalytic materials for cathode fabrication are Pt and C, the latter usually used in the form of carbon soot, deposited by passing the substrate over a candle light, or by carbon paste deposited by doctor blade, screen printing or spin coating.

Pt can be deposited by physical vapor deposition (sputtering) which gives a better quality film and precise thickness control. Pt pastes are also commercially available and can

be applied by the same techniques as carbon pastes. For this work, it was chosen to use Platisol T/SP from Solaronix [35], a platinum paste.

In this work, the first Pt paste applications were done using doctor blade technique with a microscope slide as a squeegee and scotch tape as spacer [31]. But the obtained Pt films were too thick and exhibited several dark spots. Since TiO_2 paste application via screen printing was successful, it was tested the same technique for Pt paste deposition, which was also more practical, more precise, cleaner and faster than doctor blade.

To evaluate the most efficient Pt layer thickness, meshes were tested in batch 20200223. The performances of the best cells obtained can be compared in Table 5.8.

Mesh	**V_{OC} [mV]**	**J_{SC} [mA/cm^2]**	**FF**	**η**
51HD	533	0.407	67.40%	0.15%
61HD	563	0.479	71.04%	0.19%
77HD	544	0.503	71.17%	0.19%

Table 5.8: Batch 20200223. Comparison of meshes for Pt film deposition (best cells performance).

After the above batch fabrication, other tests were done using 140HD mesh. Despite the superior results, even better than 61HD and 77HD, the cleaning process of 140HD mesh was too difficult due to the small open area and ease to clog.

Since 77HD offered the best results for both, anode and cathode, TiO_2 and Pt pastes could be printed at the same fabrication step, using the same screen, which made the fabrication process simpler and faster.

Despite the above coincidence, it could be noticed that if Pt film was thinner, the cells performance would be better, although the limitation by the utilized technique. Probably, a thin film of Pt deposited using other technique, e.g.: sputtering, would provide better results, as conducted by many other researchers. However, this approach would be out of the scope of the present work.

Protocol definition → Screen printing Tegape® 77-63 HD mesh for Pt layer deposition (77 threads/cm and 63 thread diameter)

5.2.5.3 Sintering

As presented in the last sections, Ti-nanoxide T/SP [34] and Platisol T/SP [35] pastes from Solaronix were used for TiO_2 and Pt layers deposition, respectively. The sintering temperatures and times for both pastes processing can be seen on Table 5.9, as recommended by the manufacturer.

Paste	**Sintering**	
	Temperature	**Time**
Ti-nanoxide T/SP (Solaronix)	475ºC	30 min
Platisol T/SP (Solaronix)	450ºC	10 min

Table 5.9: TiO2 and Pt pastes sintering temperature and time as recommended by the manufacturer.

Since the temperatures were close, and after checking the temperature profiles published elsewhere, it was decided to sinter both electrodes (anode and cathode) together (Figure 5.6), with the same profile, as presented in Table 5.10. This decision helped to highly reduce the overall fabrication time, since the heating and cooling ramps took a precious time, specially considering that in this work, NDSSC were fabricated and tested in the same day to avoid degeneration. This way, anodes and cathodes were completely fabricated side by side, from substrates cleaning to paste depositions and sintering.

Step	**Temperature**	**Time**
Pre-heating (drying/relaxing)	125ºC	30 min
Heating ramp	125ºC – 500ºC	~3 min
Sintering	500ºC	40 min
Cooling ramp	500ºC – 60ºC	45 min

Table 5.10: Sintering temperature profile.

The sintering temperature and time were higher than the recommended by the pastes manufacturer. This decision was taken due the reduced hotplate dimensions and heat losses.

The pre-heating step was added to guarantee a better accommodation of the paste on the substrate surface and solvent evaporation. The benefits of this step could be visually confirmed, since the pastes were smoother before sintering step.

Figure 5.6: Substrates sintering.

A very important step to be taken after sintering is letting the substrates slowly cool down back to ambient temperature. If taken too fast from the hot plate, due to differences on materials heat dilatation, the deposited films may crack and peel off. When the heating time is up, it is necessary to let the substrates cool down slowly before taking them out. For the laboratory and equipment conditions of this work, the substrates took about 45 min to cool down from 500ºC to 60ºC.

5.2.6. Anodes sensitization

5.2.6.1 Dye extraction

The chosen solvent for the present work was ethanol. During the first batches fabrication, water and ethanol were tested, both seemed to work and subject to optimization. However, ethanol better dissolved the fruit extracts and made filtration process much easier.

After solvent selection it was time to define the ratio between fruit weight and ethanol added before blending. Batch 20191217 was dedicated to this task. A total of 6 cells were

fabricated and characterized, all of them with the same fabrication methods, except the volume of added solvent. Table 5.11 shows the best cells performances.

Cell	Fruit/Solvent	V_{OC} (mV)	J_{SC} (mA/cm^2)	FF	η
1	50g / 75ml	524	0.374	64.21%	0.13%
2	50g / 50 ml	533	0.428	65.02%	0.15%
3	50g / 25ml	532	0.334	62.87%	0.11%

Table 5.11: Best cells obtained in batch 20191217.
Different fruit weight / solvent volume ratios.

After batch 20191217 fabrication, it was decided to use the ratio between fruit weight and ethanol volume of 50g/50ml or 1ml of ethanol added for each 1g of blackberry before blending.

Protocol definition → 1g/ml (fruit:solvent ratio)

5.2.6.2 Dye purification

It was tried to use vacuum filtration to separate the liquid from extract main solid parts, this procedure proved to be difficult for some solvents depending on the boiling point, since evaporation can be highly fastened by the lowering of the pressure.

Filtration also needs a reasonable solubilization level or the extract will get stuck on the paper filter and make impossible the dye extraction. Thus, solvent volume added to the extract must be carefully defined.

Besides filtration, centrifugation is an important procedure to be taken. It removes most of the solids small enough to pass through the paper filter, which would compromise the dye adsorption and electrolyte penetration inside the TiO_2 layer porous, as discussed in section 3.3.2.

Batch 20200213 was used to check the impact of centrifugation on the cells efficiency. Keeping all the other parameters, some cells were fabricated with and without centrifugation used after filtration. The obtained best cells performances can be seen in Table 5.12.

Purification	V_{OC} [mV]	J_{SC} [mA/cm^2]	FF	η
Filtration	584	0.300	74.03%	0.13%
Filtration + Centrifugation	564	0.384	76.81%	0.17%

Table 5.12: Batch 20200213 fabricated to check the impact of extract centrifugation on the cell efficiency.

It is clear the significant impact (+31%) on cells efficiency by the use of centrifugation along with dye filtration.

Protocol definition → Dye purification by filtration and centrifugation

5.2.6.3 Sensitizing

Sensitizing consists of soaking the anodes in dye solution for some time, so dye molecules can be adsorbed by TiO_2 surface. This mechanism was discussed in sections 2.2.3 and 3.4. Besides the dye solution preparation, researchers can also control two variables during sensitizing process, time and temperature. In this work, temperature were not studied, although this may be subject of future works. However, time is largely different among authors preferences, as seen in Table 5.1 and reference [8][4][6].

Batch 20190908 was one of the first fabricated in this work. It was used to compare 1h and 4h sensitizing times. Table 5.13 shows the best cells performances obtained. Differently from later batches, due to laboratory limitations at the time of this experiment, cells were characterized without the light concentration lens, and thus, under 208 W/m^2 irradiance (same xenon lamp spectrum) which justifies the much lower current if compared with cells from other batches.

Sensitizing time	V_{OC} [mV]	J_{SC} [mA/cm^2]	FF	η
1 hour	444	0.116	65.34%	0.16%
4 hours	414	0.097	59.52%	0.12%

Table 5.13: Batch 20190908 (under 208 W/m^2). Comparison of cells fabricated with 1h and 4h sensitizing times.

By the obtained results and considering that prolonged sensitizing times would make impossible the fabrication in the same day, it was decided to fix sensitizing time to 1h.

Protocol definition → Sensitizing time of 1h at ambient temperature

After sensitization, the anodes were washed with acetone to remove the excess of dye solution. Acetone was chosen because of its fast drying at ambient temperature and the electrolyte solubility in this solvent, which facilitates electrolyte penetration if some wet spots still remained prior to assembling.

5.2.7. Electrodes joining

Cells assembling comprised the electrodes joining, sealing, electrolyte injection and finally the metal contacts attachment. In the present work experiments this was far the most difficult task. The search of a practical and effective way to put everything together on a working cell was very time consuming, with several trials.

Many research groups assemble the cells simply putting together the electrodes with a few drops of electrolyte in between and fixing the set with paper binders. This procedure is also described in [31]. This technique is quite effective if the measurements are done right after assembly, since the evaporation of the electrolyte and other degeneration mechanisms can be neglected for this time frame.

However, after the first batches, it was noticed a few disadvantages: electrolyte evaporation left a short time for cells characterization, specially for batches with many cells, assembly was not very robust and the paper binders made the cell attachment to the testing board in the solar simulator more difficult. Thus, other way to assemble the cells had to be found, which will be presented in the next section.

5.2.7.1 Joining electrodes and sealing

After the electrodes are ready, the cells must be assembled by joining the two parts tightly, preventing the electrolyte leakage.

Besides the use of paper binders, UV cured epoxy was tested. The idea was to easily seal the cell with a few drops of sealing epoxy, right after assembling, on the substrates edges and above metal contacts. This procedure should have enough mechanical strength to keep all cell parts firmly attached to each other. As well, the interfaces would be well sealed avoiding leakage of the electrolyte.

The first UV curing epoxy tested was Epoxy E131 from Ossila®. To determine the

time for curing, it was used a simple commercial curing UV system with compact UV lights to cure a few drops on a sample substrate. Every 5 min the hardness of the applied epoxy was tested. The goal was to reach enough hardness to take the futures cells out directly to be measured, without further assembling procedures. It was found 30 min as an ideal time for curing.

Industrial crystal UV resin was also tested. This product showed advantages over Epoxy E131, such as: faster curing time and lower cost.

During tests with both products, one concern was the possible active film damage by UV light. But no damage was detected. The cells tested before and after the UV exposition did not show significant differences, probably by the poor UV component of this type of lamps. The same was found covering the substrates with tape to protect the photoactive area.

Despite the excellent advantages, specially mechanical strength and ease to use, both options used were not effective. Leakage could be detected in all cells fabricated in the next day using this method. So other sealing methods were tried.

DSSCs can be assembled using sealing film gaskets, Solaronix® offers an interesting option called Meltronix® [37]. However this film requires a temperature around 100ºC to seal, which was a concern since it was assumed that natural dyes could degenerate in this temperature. Turturica et al. [38] studied the thermal denaturation of anthocyanins over the time for different temperatures. It could be noticed by their reported results, a drop in anthocyanins concentration of more than 20% in just a few minutes at the temperature level necessary for Meltronix® sealing. Despite the fact that sealing process could be done in just tens of seconds, other concerns arose, like the possible weakening of the dye-TiO_2 bond and possible changes regarding the dye molecules. In the future, this sealing option will definitely be further studied and tested to check this hypothesis.

The alternative used in the present work as adhesive and sealant was Parafilm® [57]. This product is manufactured by Bemis® (recently acquired by Amcor®) and used to protect content in laboratory glassware. It consists of a flexible, semi-transparent and self-sealing film made of a blend of waxes and polyolefins. Parafilm® works as a moisture-barrier with the advantage of low softening temperature, 54ºC [57]. Thus, cells were sealed pressing the electrodes with a layer of Parafilm® in between over a hotplate set to 50ºC for 40 seconds. A hole a little bigger than the active area was opened on the film using a paper hole puncher to open space for the electrolyte (Figure 5.3). The sealing was not perfect, electrolyte evaporation could still be noticed in a few days, but it gave enough time and robustness for cells characterization.

5.2.8. Electrolyte injection and holes sealing

During fabrication protocol development, a few ways to inject electrolyte were tried. Such as putting a few microliters of electrolyte over one electrode and then close the cell with the other. This did not work since electrolyte easily leaks over the spacer layer. Using one

hole to inject electrolyte after cell sealing is impossible because the air inside pushes the electrolyte back. Some authors used a small vacuum chamber to suck the air out of the cell, and then, after pressure is released, electrolyte is sucked in. The latter method was effective but requires a careful control of the vacuum level to avoid electrolyte evaporation and the "kick" when pressure is released can flip the cell. Thus, for the present work, the way that best suited the needs was drilling 2 holes on the cathode, close to (but not over) the active area. After sealing with Parafilm®, each cell was hold with one of the sides up, in a way that holes stay one above the other. Using a micropipette, about 20µl of electrolyte was injected in the lower hole, while the air escaped from the upper hole. The cell could be inclined to the sides so any remain bubble could be pushed out while electrolyte filled the space between electrodes.

After electrolyte injection, the holes and the surfaces were cleaned using acetone and a cleanroom swab. Another layer of Parafilm® was placed over the holes, and then a coverslip on top of it. The set was again pressed by hand over the hot plate for 40 seconds at 50ºC.

The cells are then ready for metal contacts attachment.

5.2.9. Metal contacts attachment

The last step of cells fabrication was the metal contacts attachment. Alternatively, ultrasonic soldering iron could be used to deposit tin based alloy directly on substrates TCO surfaces. However, the chosen option was the "electrical connection legs for ITO glass substrates - E241", from Ossila® [39]. These connectors have clips that attach do the glass substrates just by applying pressure. The legs are spaced by 0.1 inch (2.54 mm) which make them compatible with the commercial standard for circuit boards and connectors, and thus, compatible with the home made solar simulator testing board described in section 5.4.10.1.

The E241 connectors were designed to have a leg for each individual PV cell or LED, but since unpatterned substrates was used, each side of the cell had several points of contact. The testing board in the solar simulator also connects them on each side, leaving one single electrical connection for each electrode (anode and cathode). This helps to collect as much current as possible and overcome imperfections on the substrates surfaces or on each point of connection between the substrates and the metal contacts.

The technique worked fine, but some cells were lost during assembling, because the force needed to push the cell into the E241 clips may cause the cell disassembled. This could be avoided with a carefully sanding of the substrates edges, making them easy to slide into the clips, and of course, a good adhesion between the electrodes and the Parafilm®, making all the parts firmly joined.

The E241 connectors made the characterization much simpler and practical, avoiding the need of alligator clips to electric connect the cells to the measurement equipment.

5.2.10. Characterization

Electrical measurements and other types of characterization are crucial to check hypothesis, understand increases or decreases on performance and make comparisons between different devices. Only with a stable and reliable testing setup it is possible to measure the impact of each development step taken.

On the other hand, it is necessary to consider the goals, available time and budget for the research being conducted. Practical aspects such as the estimated time for each batch fabrication and tests must also be considered. Finishing the cells or leaving characterization for the next day could compromise the quality of the results. In natural dye-sensitized solar cells the hurry to measure performance is always present since the low stability can impact the efficiency in a short time. Thus, it was decided to fabricate small batches within 6 to 8 hours (this author worked alone all the time).

Considering all above, it was chosen to focus this work devices characterization on obtaining JxV curves under 100mW/cm^2 irradiance, overall power conversion efficiency, dye absorption spectrum and visual inspection, using the following setup:

- Home made solar simulator (described in the next section)
- Ossila® X200 Source Measure Unit for JxV curves measurement.
- Stellarnet® Black-Comet-C-SR 200-1080 nm spectrometer for irradiance and dye absorption spectrum (also used for films thickness measurement)

The JxV curves measurement methodology consisted of turning the solar simulator on and monitoring the light spectrum and intensity via spectrometer until stabilization. It could be used a reference silicon cell for this step, but the spectrometer was available and easy to integrate in the solar simulator.

After stabilization, the cells were placed in the solar simulator and the JxV curves were taken. For all batches, cells were measured one after another right after assembly.

Then, the absorption spectrum of the dye solution used for sensitization were also measured using a Stellarnet® CUV1 cuvette support connected via optic fibers cables to the spectrometer.

All obtained data was saved in computer for later analysis.

5.2.10.1 Solar simulator

The design and fabrication of a solar simulator for the new constructed laboratory was an important part of the present work, not only because of the investment and time dedicated to this project, but to achieve the goal of making DSSC research more accessible to new researchers and institutions. Thus, this section will discuss this topic more deeply.

Esen et al. [14] synthesize information from several publications and state that solar simulators are important equipments, an integral part of JxV measurements because they

provide a reproducible and reliable light condition, usually the so-called Standard Test Conditions (STC) which corresponds to 1000 W/m^2 (100 mW/cm^2) irradiance, air mass (AM) 1.5 spectrum and device temperature of 25ºC. These conditions are not easily and often achieved outdoors. So, the use of a solar simulator inside the laboratory is so important.

Solar simulators are classified by their performances following the standards: American Society for Testing and Materials ASTM E927-10 and the IEC 60904-9 of International Electrotechnical Commission. Both determine ranges of performance (A, B and C) for 3 parameters: spectral match, spatial non-uniformity and temporal instability [14][40].

Just scratching the surface, it could be explained that spectral match corresponds to how close the solar simulator spectrum is to solar spectrum. Spatial non-uniformity is related how consistent the irradiance is for different points on the surface illuminated by the simulator and temporal instability indicates how stable the irradiance is over the time.

Due to high cost of professional solar simulators on the market, but at the same time, the high necessity of this equipment for the present and future works, it was decided to design and fabricate an unit of this equipment. The main target parameters considered during design were: spectral match and temporal stability. For the limited dimensions of the available sensors and fabricated DSSCs active area, the spatial uniformity parameter was not considered.

It was also part of the target characteristics of this project: low cost, user safety, ease to use and fast operation.

Light source

The solar simulator most important part is the light source, its characteristics as light intensity and beam angle will determine the internal geometry of the equipment. Efficiency and total irradiance will define the cooling system demand. The spectrum indicates its efficacy or the need of complementation by other light sources, and so on.

As well pointed by Tawifik et al. [41]: “Light source selection is the principal step designing a solar simulator with suitable solar radiation”. Thus the first step was deciding the light source technology, and most precisely, the lamp to be used.

A study of common light sources technologies applied in solar simulators was presented by Esen et al. [14]. Similar study was done by Tawfik et al. [41] but focusing on solar simulators for thermal applications. Both groups indicated advantages and disadvantages of each light source technology. Among the options, two technologies seems to be interesting, considering several characteristics, specially their light spectra: xenon arc lamps and LEDs, although tungsten halogen lamps were also tested for comparison in this work.

LED

Due to the high efficiency, small size, fast operation, good stability and market availability, LED was the first choice. The limited spectral range would be compensated by

the use of different wavelengths LEDs.

Simulations were conducted to estimate the spectrum generated by several LEDs from different colors, different viewing angles and irradiance. Similar work was done by Novickovas et al. [40] on the design of all-LED, AAA, solar simulator, which initially inspired this work to the same direction, however the disadvantage of the strategy used by this group was to focus on the total amount of irradiance generated for each wavelength range and compare with the same value from the solar spectrum. This way, one high peak on the center of the range compensates possible low values on the edges of the same range. In the end, the range total irradiance corresponds to the Sun, but for each individual wavelengths the differences could be very high. For the present work it was intended to design a solar simulator generating a spectrum curve following the Sun's, as close as possible for each individual wavelength in the visible range.

During the research of available LEDs on the market, it was found a very interesting and new white LED technology which could replace most of the necessary dozens different LEDs colors, and of course, all needed circuitry to control each color string. Usually white LEDs do not exhibit a true “full spectrum”, but often a high peak near blue and a wider but lower emission between green and yellow. This kind of spectrum creates a visually “white effect” but do not cover all visible region of the solar spectrum. However, the mentioned interesting white LED was fabricated by Yuji International and used a violet LED to excite dyes which emit light in virtually any color. The Yuji VTC ultra high CRI LEDs [42] are able to cover most of the solar spectrum with very good color balance. A lamp designed and fabricated in the present work using this LED can be seen in Figure 5.7, it contains several of these LEDs (model YJ-VTC-135L-G01). The measured spectrum can be seen on Figure 5.9. Despite of the excellent performance, it would still be necessary to complement the light source with other LEDs for the Blue-UV range and Red-IR range. Due to this fact and the time to be dedicated on the development of current drivers and power supplies, which was not in the scope of the present work, it was considered other light sources.

Tungsten halogen lamps

Tungsten halogen lamps is a type of incandescent lamp which contains halogen gas surrounding a filament of tungsten heated by electric current, as summarized by [41] from other sources. This light source was considered due to its low price and high output but it exhibits poor response on the blue and near-UV range, as seen in the spectrum obtained for each tested lamp (Figure 5.9). Even the model Osram Cool Blue Intense, which is a little shifted to blue, did not achieve an acceptable spectrum for this project.

Xenon arc lamps

Tawfik et al. [41] listed many publications reporting the use of xenon arc lamp as a light source in solar simulators, suggesting those lamps as often preferred. Esen et al. [14] also stated: “Today, the light sources in solar simulators are typically xenon arc lamps and LEDs”.

The xenon arc lamp tested was Super Vision® HID Xenon 1B15 6000K 35W, which spectrum can be seen on Figure 5.9.

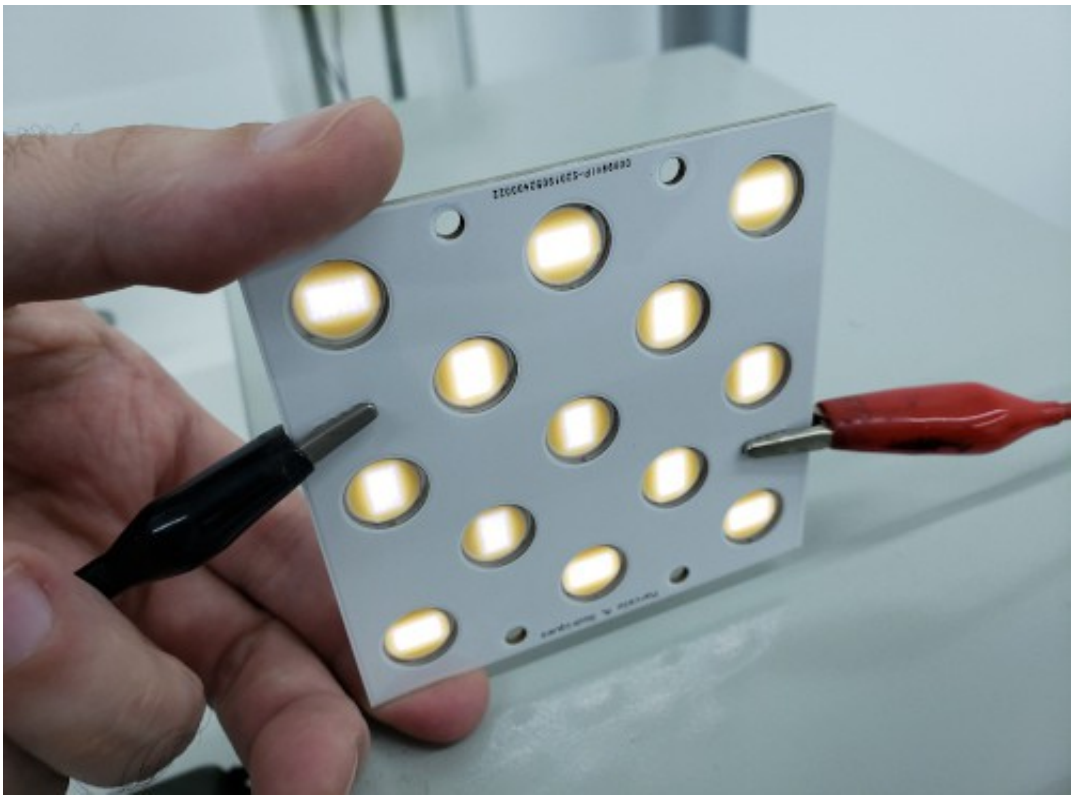

Figure 5.7: Lamp fabricated with white LEDs
Yuji International® model YJ-VTC-135L-G01.

Lamp selection

As previously indicated, one of the most important characteristic considered for this solar simulator project was the spectrum. It was intended to reach a light spectrum as close as possible to the Sun's. Thus, to evaluate the performance of the tested lamps, data from "Reference Air Mass 1.5 Spectra – NREL" [43], was compared with the spectrum measured of each light source at a few centimeters distance using a Stellarnet® Black-Comet-C-SR 200-1080 nm spectrometer with CR2 UV-Vis-NIR cosine receptor. The obtained results can be seen on Figure 5.8.

It was clear that the Xenon arc lamp could provide a spectrum close enough to the Sun's, covering a wider range of wavelength and also the AM1.5 spectrum shape. Considering the efforts necessary to develop a driver for the home made white LED lamp and the necessary light source complementation for wavelengths close to UV and IR, also considering the poor tungsten halogen lamp spectrum quality for this application, it was decided to use the xenon arc lamp.

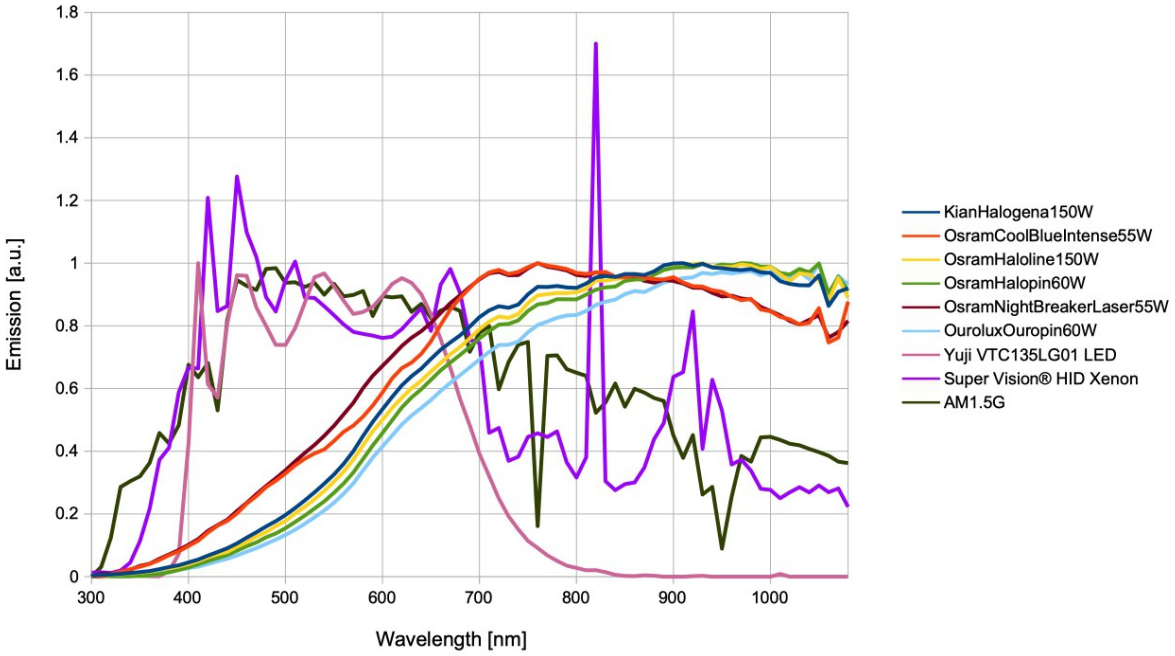

Figure 5.8: Lamps spectra versus AM 1.5 spectrum.

This lamp was designed for automotive application, so it is sold as a kit to be installed in cars. This characteristic made the project very simple, because with just a good DC power supply it would be possible to power the lamp. The included driver in the kit did all the work, starting the lamp and keeping its output reasonably constant, which could also be measured with the spectrometer. The total irradiance variation was within ±3% range, just a couple of minutes after the lamp started, which was good enough for the goals of this work.

Lenses and irradiance control

One disadvantage of the selected xenon arc lamp was its limited output power. The irradiance, just a few centimeters from the lamp was around 200 W/m^2, which is not enough considering STC conditions (1000 W/m^2). Instead of changing the lamp to a more powerful and much more expensive option, the problem was solved with a set of 2 fresnel lenses. The lenses capture the light irradiated by the lamp and concentrate it, forming a cone in the direction of the cell. This also permitted the irradiance control, since in this project the distance between the sample and the lamp/lenses is adjustable, and so the irradiance intensity. More details of the set of lenses and light source are seen on Figure 5.9.

With the use of both resources: distance adjustment and concentrating lenses, it is even possible to reach an irradiance over 3000 W/m^2, which may be also useful for future concentrating PV studies.

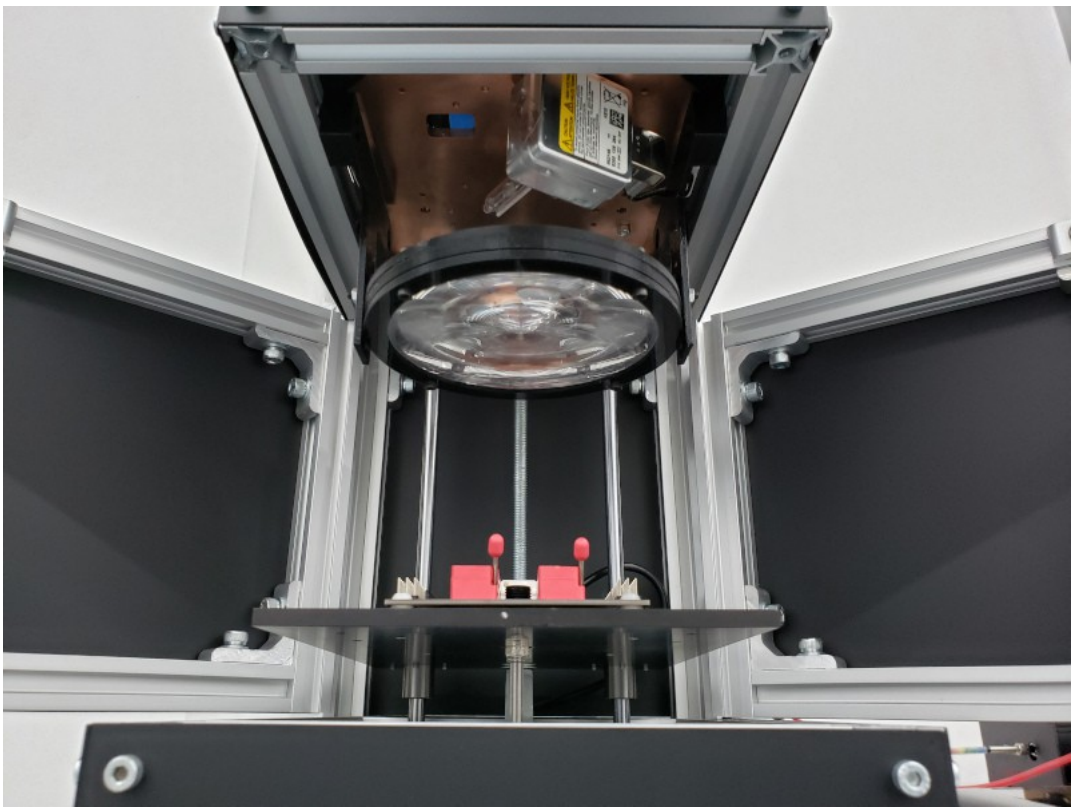

Figure 5.9: Pictures of the lenses set and light source.

Design

The fabricated solar simulator design was simple. Internally, a printed circuit board (cell board) had ZIF contacts with two small levers to tightly hold the solar cell contacts, this proved to be a good resource because it was very easy to fix the cell, and changing the levers position, the cell stayed firmly held with a good electric contact. The cell board also had a soldered BNC cable connector, to connect the JxV measurement equipment. The cell board could be configured to select each solar cell pin independently. For this work, since each sample has only one cell, all pins of each side were short circuited by jumpers, providing a better current measurement.

The cell board was fixed with plastic screws to a black aluminum base attached to a set of 2 linear bearings and shafts. The base height could then be adjusted by manually rotating a nut attached to a rail.

All the above parts were fixed in a box made of extruded aluminum covered with black aluminum plates, all parts were designed using Fusion 360® software from Autodesk® and manufactured by local suppliers. The upper part of the box was ventilated and isolated, it held the temperature monitoring circuitry, the lamp driver and cooling system, which was done with a computer chip cooler in contact with a copper plate, where the lamp was attached. The air was sucked from the solar cell chamber up to the isolated box and then to the back of the equipment.

The equipment upper panel had a digital display showing the copper plate temperature. Two doors on the front side gave access to cell board from a wide angle. A picture of the finished solar simulator can be seen in Figure 5.10.

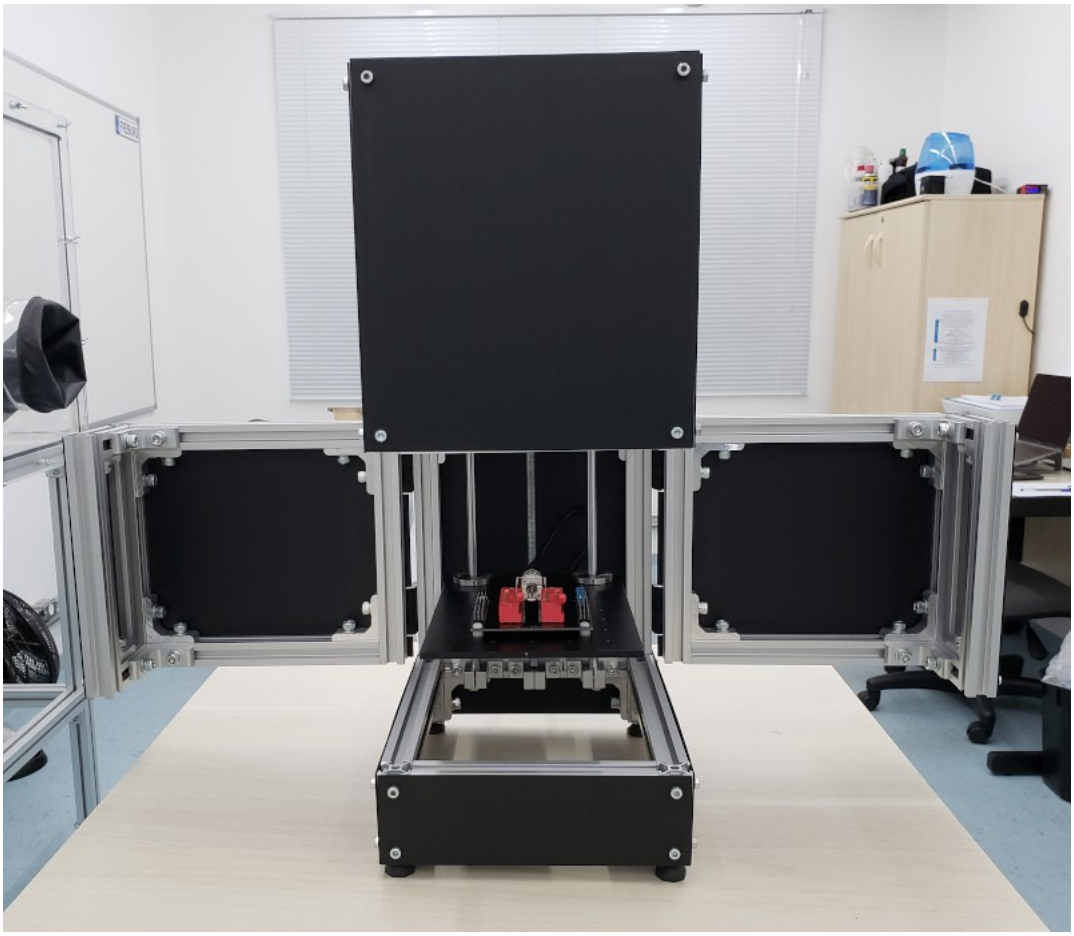

Figure 5.10: Picture of the finished solar simulator.

5.2.10.2 JxV curve

The IxV curves was obtained using the solar simulator cell board connected to an Ossila® Source Measure Unit (X200), this equipment has several configuration options including sensitivity, voltage and current ranges, reading speed, among others. The generated curves were saved in the computer for later analysis. Each current point was later divided by the active area (A = 0.2827 cm^2) to transform the curve to its current density versus voltage (JxV) form.

5.2.10.3 Absorption spectrum

After each cell batch fabrication, the dye solution absorption spectrum was also studied. The equipment used was the Stellarnet® Black-Comet-C-SR 200-1080 nm spectrometer, a 5W Tungsten Krypton 2800K light source and CUV1 cuvette support all connected by optic fibers.

Absorption spectrum of each dye is important to recognize the pigments present. This procedure was used by Singh et al. [24] to find anthocyanins in the extracts of *Begonia malabarica, Melastoma malabathricum* and *Punica granatum* by strong absorption spectrum peaks (543 nm, 535 nm and 520 nm respectively). Chlorophyll also was identified in *Begonia malabarica* by peaks in 444 nm and 681 nm. The present work used similar observations to recognize the pigments groups in the extract of each species used. More details can be found in section 6.1.6.

5.2.10.4 Data analysis

Data obtained from the JxV curves were exported to Open Office Calc software. By the method described elsewhere [13], for each curve it was taken the following values:

V_{OC} (Open circuit voltage – voltage when current is zero in the curve)
I_{SC} (Short circuit current – current when voltage is zero in the curve)
MPP (Maximum power point – point on the curve where VxI is maximum)
V_{MPP} (Voltage at maximum power point)
I_{MPP} (Current at maximum power point)

Fill factor (FF) and overall conversion efficiency (η) were calculated using formulas 2.4 and 2.6 (section 2.1.1). As seen in previous sections, all fabricated cells in this work had the same active area, A = 0.2827 cm^2.

5.2.10.5 Thickness measurement

Thickness measurement of TiO_2 layer was also an important tool used for cells performance optimization. The used technique was described in [44]. With a spectrometer it is possible to observe the interference pattern created by the interaction of a light beam being reflected on the film deposited over a substrate. It was used the spectrometer Stellarnet® Black-Comet-C-SR 200-1080 nm with R600-8-Vis-NIR reflectance probe and RPH3 support, along with a 5W Tungsten Krypton 2800K light source. The Stellarnet® TF-STD1 with thickness standards was also used to test the method.

The light beam was projected on the substrate surface out of the deposited layer, and the observed spectrum was saved. Right after, the light beam was projected over the deposited layer and the absorption function of the spectrometer software was used to subtract both spectra and exhibit the interference pattern. A wavelength range with pronounced and well defined peaks is chosen, the starting and ending wavelengths of the range is noted, along with the number of peaks within the chosen range. The noted information is then applied to the formula 5.1 for the thickness calculation. The equipment setup can be seen in Figure 5.11.

Figure 5.11: Spectrometer setup used for thickness measurement

$$d = \left(\frac{\Delta m}{2\sqrt{n^2 - \sin^2\theta}}\right) * \left(\frac{1}{\left(\frac{1}{\lambda_2} - \frac{1}{\lambda_1}\right)}\right) \tag{5.1}$$

Thickness calculation is done using the formula 5.1 [44], where:

d is the layer thickness;
Δm is the number of peaks in the wavelength range being considered;
n is the refraction index of the layer material;
θ is the angle of incidence (0º if vertical incidence);
λ_2 and λ_1 are the start and end wavelengths of the range being considered.

The above procedure was first used with a SiO_2 1μm deposited layer over silicon from the TF-STD1 standard. The obtained result confirmed the effectivity of the method.

The obtained results for the 1μm SiO_2 standard used are shown in Table 5.14.

Δm	**n**	**θ**	**λ_1**	**λ_2**	**d**
4	1.46 [45]	0º	778nm	361nm	0.923μm

Table 5.14: Parameters used for thickness calculation of SiO_2 1μm standard.

As can be verified in Table 5.14 the obtained value for the standard was 0.923 μm, close enough to 1 μm, the real film thickness as informed by the manufacturer. Thus, the above thickness measurement technique was chosen for the characterization of the anodes fabricated in the present work, taking the care of using the appropriate refraction index for TiO_2 mesoporous film, which is 2.11 [46].

5.3. Fabrication protocol summary

All the studies and experiments presented above are summarized it in Table 5.15 which shows, step by step, enough details for any interested researcher to follow, and certainly, improve by his/her own experience. It was very satisfactory to notice, by the results described in section 6, that the obtained cells by this protocol exhibited low parameters variability and acceptable performance. Specifications of the materials and equipments utilized in the procedures described in the protocol can be found in Table 5.16 and 5.17 respectively.

Fabrication Protocol of Natural Dye-Sensitized Solar Cells	
Procedures	**Materials and Equipments**
Step 1 – Preparing substrates (day before)	
• Check conductive side of each substrate with a multimeter • Drill cathode holes (DI water drops to wet the driller tip) • Sand substrates edges (do not scratch substrates surfaces) • Check conductive sides again • Sonicate in alkaline detergent solution – 20 min @ 40ºC • Wash in DI water 4 or 5 times • Cut Parafilm® sealing gaskets (square with a hole for the active area)	• FTO substrates • Multimeter • Driller and diamond tip • Sandpaper 220 grit • Ultrasonic bath • Alkaline detergent solution • DI water • Parafilm® M • Paper hole puncher
Step 2 – Cleaning substrates	
• Sonicate in alkaline detergent solution – 10 min @ 40ºC • Wash in DI water 4 or 5 times • Sonicate in acetone – 10 min @ 40ºC • Sonicate in ethanol – 10 min @ 40ºC • Clean screens for screen printing (carefully with acetone) • Clean 2 petri dishes set with ethanol • Number each substrate position for future reference	• Alkaline detergent solution • DI water • Acetone • Ethanol • Screen 77-63 mesh • Petri dishes • Pen
Step 3 – Printing TiO_2 and Pt films	
• Fix all substrates on the template using Scotch® tape (by the edges) • Fix screen well aligned with the template • Stir TiO_2 with a glass rod • Apply TiO_2 paste close to the anodes areas on the screen • Spread the paste using appropriate squeegee (only 1 pass) • Repeat the above to apply Pt paste (avoid intense light) • Remove substrates and place in marked positions in petri dishes	• Scotch® tape • Screen printing template • Screen printing squeegee • 77-63 screen • TiO_2 paste • Pt paste • Glass rod
Step 4 – Sintering	
• Dry/Relax substrates in hot plate – 30 min @ 125ºC (in fume hood) • Sintering – 40 min @ 500ºC • Slowly cool down until 60ºC (~ 45 min) • Put electrodes back in petri dishes • Measure films thicknesses	• Hot plate • Fume hood • Thickness measurement equip.

Step 5 – Dye preparation (can be executed at the same time as step 4)	
• Weight plants • Add ethanol and plants in a blender (1g fruit : 1 ml ethanol) • Blend for 1 min. • Filter using paper coffee filter • 10 ml in each centrifuge tube • Centrifuge for 40 min @ 3000 RPM	• Scale • Ethanol • Paper coffee filter • Centrifuge
Step 6 – Sensitizing	
• Transfer the liquid part of each tube to small jars (use a dropper) • Soak 1 anode per jar, close and cover with aluminum foil • Wait for 1 hour • Rinse each anode with acetone • Wait a few minutes for drying • Protect anodes from light and humidity	• Small beakers or jars • Aluminum foil • Acetone
Step 7 – Assembly	
• Lay Parafilm® sealing gaskets on cathodes (holes aligned) • Lay anode over the gasket/cathode • Align the 3 parts and gently press • Press firmly over the hot plate for 40 seconds @ 50ºC • Inject electrolyte (20 µl) via cathode hole (avoid bubbles) • Cover both holes with a piece of Parafilm® • Place a glass coverslip on top of the Parafilm® piece and gently press • Press firmly over the hot plate for 40 seconds @ 50ºC • Attach metal contacts to both electrodes (hold firmly)	• Parafilm® • Hot plate • Electrolyte • Micropipette • Glass coverslips • Metal contacts
Step 8 – Characterization	
• Inspect cells for defects • Adjust solar simulator to 1 kW/m^2 • Measure JxV curve under illumination • Measure dye absorption spectrum	• Solar simulator • JxV measurement equip. • Spectrometer

Table 5.15: NDSSC fabrication protocol.

Fabrication Protocol of Natural Dye-Sensitized Solar Cells	
Materials	**Specification**
FTO substrates	Ossila® FTO Coated Glass (unpatterned) TEC 10, S302, 1.1mm, 9.39±0.38 Ω/□
Parafilm®	Parafilm® M, 4 in. x 125 ft., roll
Paper hole puncher	Regular paper hole puncher, 6 mm diameter circle hole
Sandpaper	220 grit sandpaper
Alkaline detergent	Borer® alkaline detergent, Deconex 15PF-x
Ethanol	Anidrol® Álcool Etílico Absoluto 99,5% PA
Acetone	Anidrol® Acetona PA ACS
Scotch® tape	Scotch® Magic 810 tape
TiO_2 paste	Solaronix® Ti-Nanoxide T/SP
Pt paste	Solaronix® Platisol T/SP
Paper filter	Paper coffee filter Melitta® Original
Electrolyte	Solaronix® Iodolyte AN-50
Glass coverslips	Ossila® Encapsulation Coverslips for PV and OLED Substrates, 12 x 15 mm
Metal contacts	Ossila® Electrical Connection Legs for ITO Glass Substrates, 1.1.mm, 6 legs

Table 5.16: Materials and equipments

Fabrication Protocol of Natural Dye-Sensitized Solar Cells	
Equipments	**Specification**
Multimeter	Minipa® ET-2082C digital multimeter
Driller	Dremel® 3000 rotary tool with table top workstation
Ultrasonic bath	Schuster® lavadora ultrasônica L200
DI water system	BWDS® osmose reversa e desmineralizador 200L/D
Screen printing template	Home made with formica-laminated wood sheet with aluminum sheet guides
Screen printing squeegee	Wood-rubber screen printing squeegee
Screen printing screen	Wood framed screen, Tegape® 77-63 HD mesh (77 thr./cm and 63 thr. diameter)
Hot plate	LGi Scientific® MS7-H550-S, 550ºC microcontrolled hot plate.
Scale	Bioprecisa® Electronic Balance FA-2104N
Centrifuge	Daiki® Centrifuga 80-2B
JxV curve measurements	Ossila® Source Measure Unit (X200)
Solar Simulator	Home made xenon lamp solar simulator with concentrator lens (section 5.2.10.1)
Spectrometer • Thickness measurement • Absorption spectrum • Irradiance spectrum	Stellarnet® Black-Comet-C-SR 200-1080 nm spectrometer. • R600-8-Vis-NIR reflectance probe, RPH3 support, TF-STD1 thick. standard • CUV1 cuvette support and 5W Tungsten Krypton 2800K light source • CR2 UV-Vis-NIR cosine receptor
Others	Glassware, micropipette 100 µl, stainless steel tweezers, etc

Table 5.17: Materials and equipments

6. Results

As seen in section 5, this work started from a fabrication protocol suggested elsewhere [31], and step by step each technique was modified and optimized to find the best performance possible in the context of the available equipments, materials, and specially, the following goals: simplicity, low cost and reliability.

The dye source used during the optimization process was blackberry fruit (*Rubus* spp), as suggested by the initial protocol [31], but also due to its natural availability in Brazil and availability in local markets.

6.1. Species selection

To fulfill the goals of the present work, other Brazilian plants should be tested. Thus, specialists from Jardim Botânico de São Paulo (São Paulo public botanic garden) were consulted. With great enthusiasm and availability, the team offered very valuable hints, advices and explanations. They also provided the samples needed for fabrication of DSSC with other species than blackberry (many thanks for this incredible support).

The idea was to have some variability of the type of plants parts used, meaning fruits, flowers and leaves, the main sources of pigments. Also, a very interesting concept offered by the specialists was to include plants largely cultivated in Brazil, even if they were not naturally originated in a Brazilian biome. Finding a plant with a well established and strong agribusiness could offer more opportunities for future research and development.

Thus, the selected plants were:

- Amora-preta / Blackberry fruits (*Rubus* spp)
- Quaresmeira flowers (*Tibouchina granulosa*)
- Embaúba-vermelha leaves (*Cecropia glaziovii*)
- Café arábica / Arabica coffee leaves (*Coffea arabica*)
- Cana-de-açúcar / Sugarcane leaves (S*accharum officinarum*)

Each of these species will be commented below, including the fabricated DSSC performance results obtained with each species.

It is important to mention that all species were used to fabricated the cells following rigidly the developed protocol (detailed in Table 5.15). However, the ratio between plant weight and ethanol volume added before blending were varied, because some plant dyes are harder to extract than others. The specific volume of ethanol added for each dye extraction are also specified below.

6.1.1. Blackberry fruits (*Rubus* spp)

Blackberry (*Rubus* spp) is found in many regions in Americas, Europe, Africa and Asia. In Brazil, this plant is naturally found in the South, specially in Rio Grande do Sul state, where is known as “amora-preta”. The plant is a bush which produces black fruits with between 4 and 7 grams each. The flavor is sweet, slightly tart, and can also be consumed as jelly, juice, ice-cream or yogurt [47]. Figure 6.1 shows a picture of this fruit still in the plant.

Figure 6.1: Blackberry (*Rubus* spp).
Picture source: Fir0002 https://pt.wikipedia.org/wiki/Amora-silvestre
(license CC-BY-SA-3.0)

Since blackberry production is easy and do not require defensive chemicals, it can be cultivated by small farmers, specially those with focus in organic food [47].

One of the most important pigments present in blackberry fruits is anthocyanin [20] [19] which is of great interest for NDSSC fabrication, as seen in section 3.1.

The fabrication of NDSSC using blackberries followed the protocol summarized in section 5.3. About 173g of fruit were blended with 173 ml of ethanol to form the extract. Figure 6.2 shows some pictures of the process.

Figure 6.2: Blackberries dye. Extract filtration (upper left), centrifugation (upper right), cells sensitizing (lower left) and fabricated cells (lower right).

The performance of the fabricated cells can be found in Table 6.1, while the dye absorption spectrum is provided in Figure 6.13.

Cell	V_{OC} [mV]	J_{SC} [mA/cm^2]	FF	η
1	584	0.535	80.14%	0.25%
2	575	0.503	80.17%	0.23%
3	584	0.531	77.61%	0.24%
			η average:	**0.24 ± 0.01 %**

Table 6.1: Performance of blackberry dye based cells.

6.1.2. Quaresmeira flowers (*Tibouchina granulosa*)

The period of lent preceding Easter is very important for the Christian tradition. In Portuguese, this period is known as “quaresma”, the word that gives *Tibouchina granulosa* tree its popular name in Brazil “Quaresmeira”, because of the spectacular violet and pink flowers produced by this tree prior and during Easter. This fast growing tree is native in the Atlantic Forest of Brazil [58]. A picture of Quaresmeira can be seen in Figure 6.3.

Figure 6.3: Quaresmeira (*Tibouchina granulosa*).

The interest to test this plant for NDSSC fabrication came from the incredible color of the blossoms, which could provide interesting cells performance.

Fabrication process followed the protocol summarized in section 5.3, but for the best dye extraction, more ethanol was used. For this plant, 12g of flower petals were blended with 72 ml of ethanol. Some pictures of the dye extraction can be seen in Figure 6.4.

Figure 6.4: Dye extraction and cells fabrication from quaresmeira flowers.
Petals (upper left), filtered extract (upper right), tubes after centrifugation (lower left) and sensitization (lower right)

Performance information of the fabricated cells can be found in Table 6.2. Dye absorption spectrum is provided in Figure 6.13.

Cell	V_{OC} [mV]	J_{SC} [mA/cm^2]	FF	η
1	564	0.401	79.23%	0.18%
2	564	0.378	80.99%	0.17%
3	555	0.369	78.71%	0.16%
			η average:	**0.17 ± 0.01 %**

Table 6.2: Performance of quaresmeira dye based cells.

6.1.3. Embaúba-vermelha leaves (*Cecropia glaziovii*)

Cecropia genus (Urticaceae), a group of 70 to 80 species consisting of native trees from Central to South America, and has been used by several traditional health treatments. Its antihypertensive, bronchodilator, hepatoprotective, axiolytic and antidepressant effects have been confirmed by research. Compounds as procyanidins, catechins, chlorogenic and caffeic acid, and flavonoids have been found in extracts of this plant [48]. A picture of "embaúba-vermelha" can be seen in Figure 6.5.

Specifically *Cecropia glaziovii*, popularly known in Brazil as "embaúba-vermelha" is 20m tall tree, common in moist forests, with green leaves upper surface and white or gray lower surface, which comes from a arachnoid indumentum covering the leaves back side [49].

Figure 6.5: Embaúba-vermelha (*Cecropia galziovii*).
Picture source: Wikipedia.org (license free).

By the so diverse and useful compounds in health treatment, this species was chosen to be tested as dye source for NDSSC fabrication. Dye extraction was done by blending 11g of leaves taken from young plants cultivated in a greenhouse with 49 ml of ethanol. Pictures of the process can be seen in Figure 6.6.

Figure 6.6: Dye extraction from embaúba-vermelha. Leaves (upper left), cut leaves (upper right), ethanol blend (lower left) and dye before centrifugation (lower right).

Performance information of the fabricated cells can be found in Table 6.3. Dye absorption spectrum is provided in Figure 6.13.

Cell	**V_{OC} [mV]**	**J_{SC} [mA/cm^2]**	**FF**	**η**
1	601	0.794	70.86%	0.34%
2	601	0.762	72.87%	0.33%
3	602	0.790	72.18%	0.34%
			η average:	**0.34 ± 0.01 %**

Table 6.13: Performance of cecrópia dye based cells.

6.1.4. Arabica coffee leaves (*Coffea arabica*)

Coffea genus comprises dozens of species. The 25 most important are all native from tropical Africa, but some are from islands of Indic Ocean, specially Madagascar. Coffee plant varies from small bushes to 10 m tall trees. The economically most important species are *Coffea arabica* (Arabica coffee), with around 60% market share, and *Coffea canephora* (Robusta coffee). Arabica coffee plant is usually a big bush with dark green leaves [50].

Coffea arabica is a shade-loving plant. Shade triggers important differences in physiological behavior, improving photosynthesis and increasing leaf area index. Coffee plants grown under shade produce larger and heavier fruits with better grown beans [51]. A picture of Arabica coffee plant is shown in Figure 6.7.

Figure 6.7: Arabica coffee (*Coffea arabica)*

Although arabica coffee, the most produced species, is not a plant originated in Brazilian territory, it was included in this work because of its high production in the country. Brazil is the biggest coffee producer in the world, with 59 millions of 60 kg bags produced in 2019 [52]. This huge agribusiness certainly could provide not only access to plants production and processing in high volumes but also being an important financial supplier for further research in this field. Thus arabica coffee was selected as one of the dye sources in this work.

For dye extraction, 40g of arabica coffee was blended with 80ml of ethanol. Some pictures of the process can be seen in Figure 6.8.

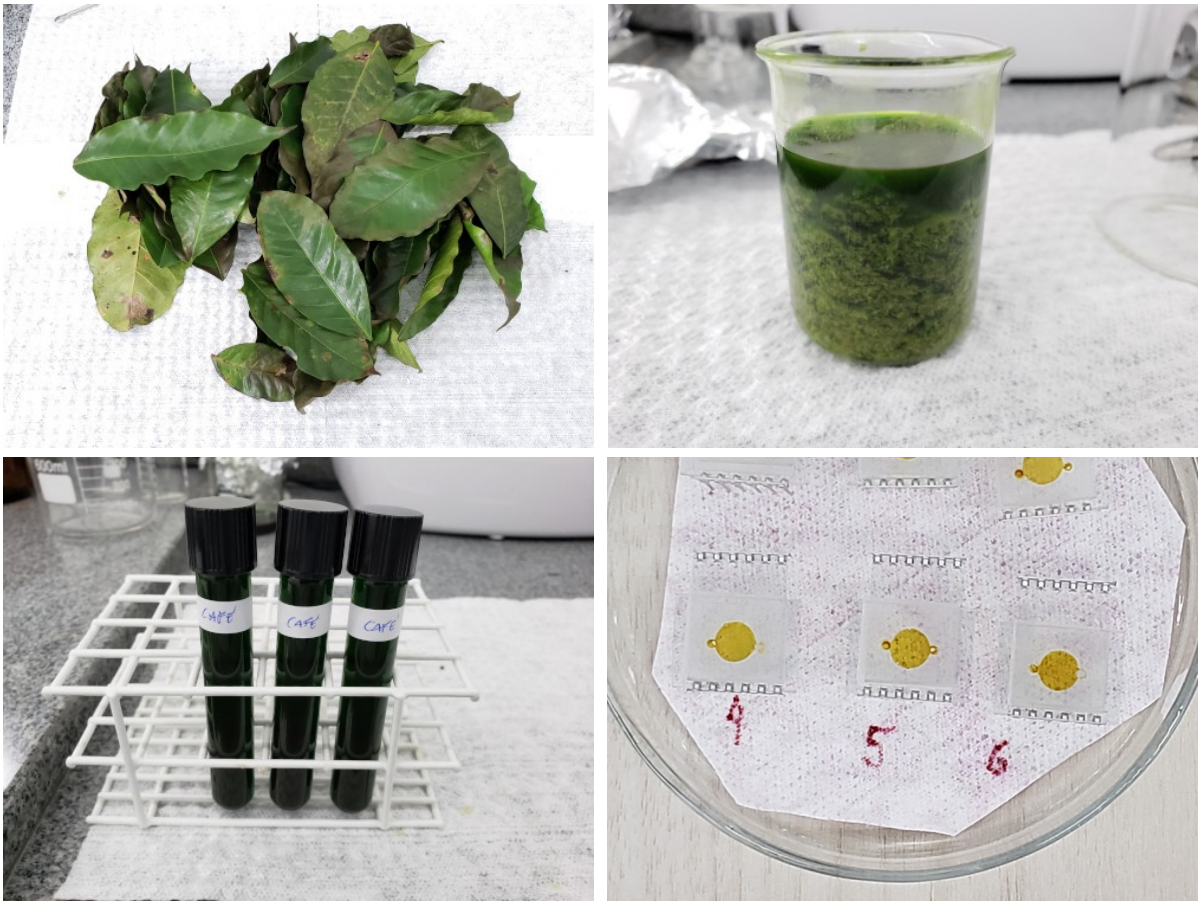

Figure 6.8: Dye extraction from arabica coffee. Leaves (upper left), extract after blending (upper right), dye centrifuged (lower left) and cells fabricated (lower right).

Table 6.14 shows performance information of the fabricated cells. Dye absorption spectrum is provided in Figure 6.13.

Cell	V_{OC} [mV]	J_{SC} [mA/cm^2]	FF	η
1	624	1.013	69.45%	0.44%
2	643	0.966	67.47%	0.42%
3	643	0.974	69.53%	0.44%
			η average:	**0.43 ± 0.01 %**

Table 6.14: Performance of coffee dye based cells.

6.1.5. Sugarcane leaves (*Saccharum officinarum*)

Sugarcane is a tall plant, reaching up to 6 m, thin and cylindrical. It is used for sugar and bio-fuel production (ethanol). A picture of the plant can be seen in Figure 6.9. In Brazil, sugarcane has a very important economical role, it reduces the dependency of fossil fuels since any gas station in the country has this alternative available, in fact, many car models are "flex", meaning they can use gasoline and/or alcohol in any mixture ratio. Also, in Brazil, gasoline must include 25% of ethanol as an octane enhancer, further reducing gasoline consumption [53].

Figure 6.9: Sugarcane (*Saccharum officinarum*).
Picture source: Hannes Grobe wikimedia.org
(license CC-BY-SA 2.5).

The world leading production of sugarcane by Brazil, associated with the fact that the sugarcane leaves are not utilized for sugar or ethanol production, may open an interesting economical opportunity for the use of those leaves in NDSSC fabrication. Also, the huge size of this industry may motivate research investments in the future.

The fabrication of NDSSC using sugarcane in this work brought a challenge. The leaves have a hard stalk, which makes the blending very hard, even if they are cut in small pieces. Also, a high volume of ethanol had to be added because the leaves sucked most of the solvent. Thus, it was used 252 ml of ethanol for 63g of sugarcane leaves for dye extraction. Pictures of the dye extraction can be seen in Figure 6.10.

Figure 6.10: Sugarcane dye extraction. Leaves (upper left), after blending (upper right), filtration (lower left) and dye before centrifugation (lower right).

Performance parameters of the fabricated cells can be seen in Table 6.15. Dye absorption spectrum is provided in Figure 6.13.

Cell	V_{OC} [mV]	J_{SC} [mA/cm^2]	FF	η
1	594	0.724	70.77%	0.30%
2	594	0.702	71.35%	0.30%
3	594	0.718	68.44%	0.29%
			η average:	**0.30 ± 0.01 %**

Table 6.15: Performance of sugarcane dye based cells.

6.1.6. Comparison of species performances

Below it is presented a performance comparison. Figure 6.11 shows the JxV curve of the best cells obtained from each dye source (plants). It is interesting to notice that arabica coffee dye achieved the best V_{OC}, but the superior J_{SC} was even more pronounced, both along with a very good fill factor, made the best efficiency of all dyes. The efficiencies comparison is better visualized in the bar graph of Figure 6.12.

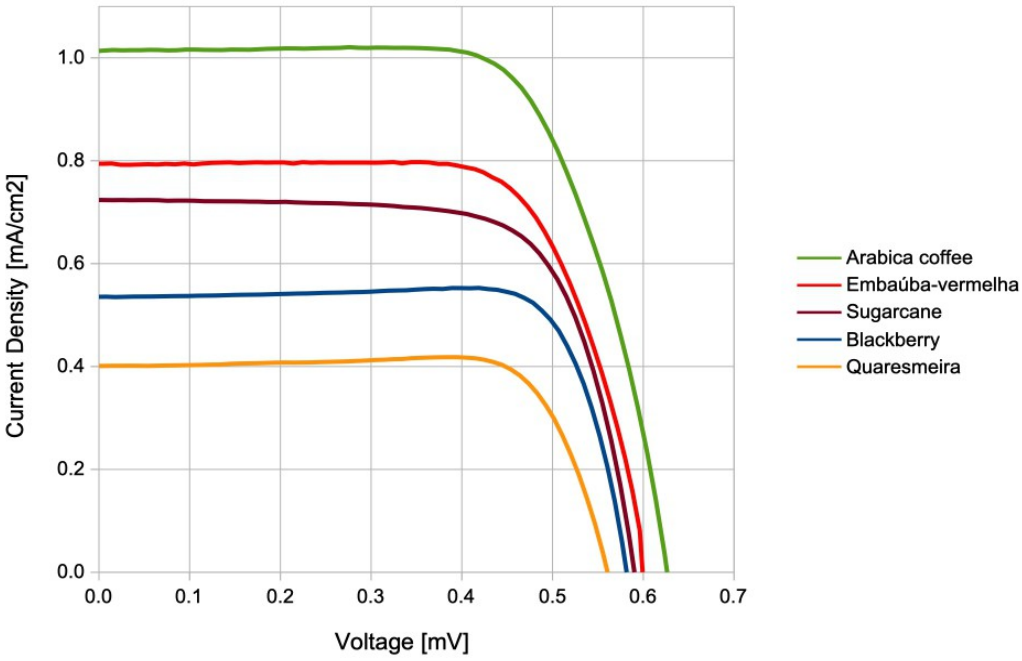

Figure 6.11: JxV curves of the best cells of each plant.

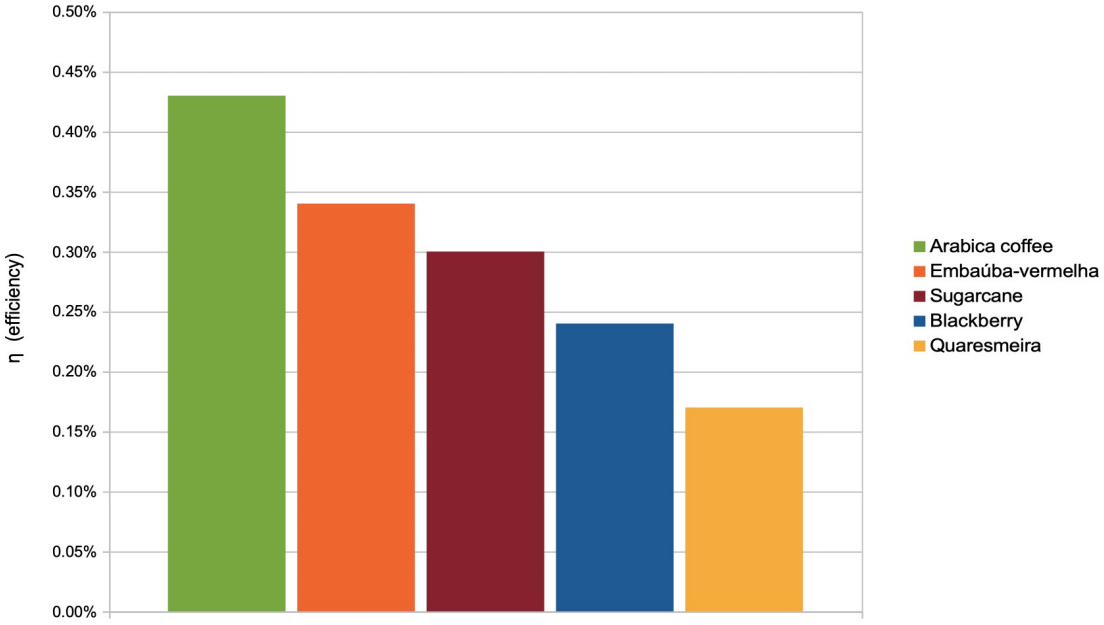

Figure 6.12: Best efficiencies achieved with each plant.

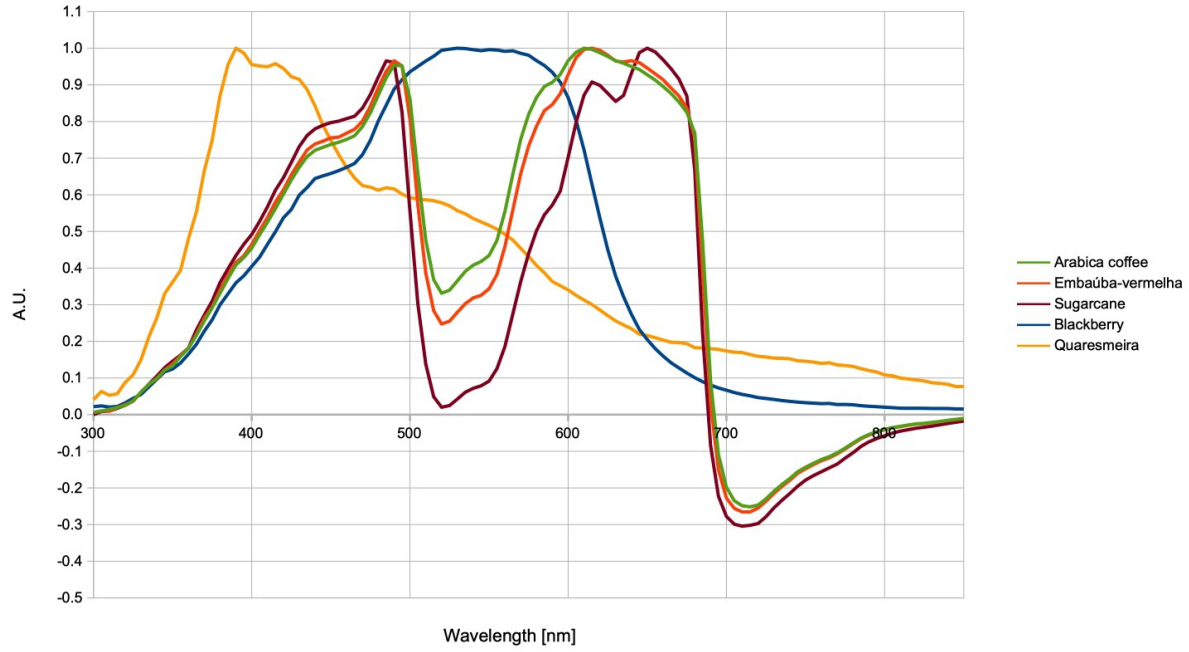

Figure 6.13: Absorption spectra of plant extracted dyes.

Absorption spectra (Figure 6.13) offer some interesting observations. At the first glance, the negative values in the range ~700-850 nm catches the attention. This occurs due the fluorescence of chlorophyll "a". The energy absorbed in UV to blue and red ranges is emitted back by the chlorophyll "a" molecules in red to deep red range [54]. This phenomenon can be observed in the three chlorophyll based dyes spectra (arabica coffee, embaúba-vermelha and sugarcane), but not in anthocyanin based ones (blackberry and quaresmeira) in which chlorophyll "a" is not present.

The above association of pigments to the plants could be verified by the observation of the spectra, that is also supported by literature. The first association (leaves → chlorophyll) is supported by the two peaks (red and blue) and incredible similarities of the studied leaves with the published work by Moss and Loomis [55].

Blackberry association with anthocyanin is obvious due several published works matching with the obtained spectrum [16][22][19][24]. On the other hand, quaresmeira association to anthocyanin is not so obvious, and it was necessary to consider the behavior of this pigment under pH variation, shifting they absorption spectrum peak, as demonstrated using the same flower by Soares et al. [56]. This peak shift is useful for pH measurements and can clearly be observed by the difference in color of the flower (blue-purple) and its extracted dye in ethanol (orange), Figure 6.2.

Another interesting observation regarding the absorption spectra is their complementarity. Chlorophylls and anthocyanins absorb light in complementary wavelengths. The mix of those pigments could offer a wider absorption range and more efficient cells. In fact, this was already explored by Sanjay et al. [9] mixing the two pigments with efficiency improvement. Iqbal et al. [8] mentioned other works with similar success on mixing different plants dyes.

7. Discussion

By the conclusion of the present work it was possible to achieve the initial goals with important learnings and findings.

Regarding the laboratory construction and equipping, it was demonstrated that a simple, but well planned, infrastructure can be used for DSSC fabrication. Climate control is crucial, humidity and temperature can highly interfere on results. A clean room can be avoided, however, space cleanliness and organization is necessary for avoiding dust or particles to be deposited on the electrodes films.

Equipments, specially for cells characterization, is also a concern. To keep costs down, spectrometer was used in different functions: measure and adjust solar simulator light intensity, films thickness measurement and dyes absorption spectrum. Solar simulator, due the high cost was home made, using xenon lamps and an aluminum enclosure. JxV curves were taken from a professional equipment, but a simple electronic circuit could also provide enough precision.

Most of this work efforts was directed to the cells fabrication protocol. The achievement of reasonable performance parameters, specially current, fill factor and overall efficiency, was not an easy task. Therefore, the performance achieved by the fabricated cells are in the range of many other research groups results in the same field, leading to the conclusion that this protocol is reliable, while still simple and cost effective.

This work aimed for the fabrication of DSSC using natural dyes extracted from plants, but synthetic dye cells could also be fabricated with a reasonable quality for research and education purposes using the same structure and methods.

Arabica coffee leaves were a pleasant surprise. Despite the fact that all optimization focus was directed to anthocyanins from blackberries, chlorophyll based extract from arabica coffee leaves gave the best efficiency, 0.44%. In the future, further development and optimization for this plant can offer even better results, in special the optimization of ethanol volume, perhaps the use other solvents and co-adsorbents, like organic acids.

It is hoped that other researchers and institutions can benefit from the present work, not only by its findings but as an incentive for others to join an even greener PV energy generation. This journey is just beginning!

8. Bibliography

[1] Jean et al., “Pathways for solar photovoltaics”, Energy & Environmental Science 8, 1200, 2015.

[2] Fraunhofer ISE, “Photovoltaics Report”, 2019.

[3] NREL, “Best Research-Cell Efficiencies”, 2020.

[4] Kumara et al., “Recent progress and utilization of natural pigments in dye sensitized solar cells: A review”, Renewable and Sustainable Energy Reviews 78, 301-317, 2017.

[5] Gong et al., “Review on dye-sensitized solar cells (DSSCs): Advanced techniques and research trends”, Renewable and Sustainable Energy Reviews 68, 234-246, 2017.

[6] Shalini et al., “Review on natural dye sensitized solar cells: Operation, materials and methods”, Renewable and Sustainable Energy Reviews 51, 1306-1325, 2015.

[7] O'Regan and Grätzel, “A low-cost, high-efficiency aolar cell based on dye-sensitized colloidal TiO_2 films”, Nature 353, 1991.

[8] Iqbal et al., “Progress in dye sensitized solar cell by incorporating natural photosensitizers”, Solar Energy 181, 490-509, 2019.

[9] Sanjay et al., “Performance of TiO2 based dye-sensitized solar cells fabricated with dye extracted from leaves of Peltophorum pterocarpum and Acalypha amentacea as sensitizer”, Materials Letters, 2018.

[10] Cahen et. al., “Nature of Photovoltaic Action in Dye-Sensitized Solar Cells”, Journal of Physical Chemistry 104, 2053-2059, 2000.

[11] Würfel et al. “Physics of Solar Cells: From Basic Principles to Advanced Concepts”, John Wiley & Sons Incorporated, Chapter 6, 2016.

[12] Han et al., “Modeling of an equivalent circuit for dye-sensitized solar cells”, Applied Physics Letters 84, 2004.

[13] Gamry Instruments, “Dye Solar Cells – Part 1: Basic Principles and Measurements”, Application Note, 2015.

[14] Esen et al., “Light sources of solar simulators for photovoltaic devices: A review”, Renewable and Sustainable Energy Reviews 77, 1240-1250, 2017.

[15] Qiao et al., “A comparison of fluorine tin oxide and indium tin oxide as the transparent electrode for P3OT/TiO2 solar cells”, Solar Energy Materials & Solar Cells 90, 1034-1040, 2006.

[16] DeSilva et al., “Broad absorption natural dye (Mondo-Grass berry) for dye sensitized solar cell”, Journal of Materials Science: Materials in Electronics, 2017.

[17] Ghann et al., “Fabrication, Optimization and Characterization of Natural Dye Sensitized Solar Cell”, Scientific Reports, 2017.

[18] Shirkavand et al., “The Construction and Comparison of Dye-Sensitized Solar Cells with Blackberry and N719 Dyes”, Journal of Optoelectronical Nanostructures Vol. 3, No. 1, 2018.

[19] Calogero et al., “Anthocyanins and betalains as light-harvesting pigments for dye-sensitized solar cells”, Solar Energy, 2012.

[20] Maged et al., “Optical Absorption Spectroscopy of the Blackberry Dye Applied in Solar Cell Sensitizers and Gamma Radiation Effects”, Arab Journal of Nuclear Sciences and Applications, 2018.

[21] Shalini et al., “Studies on DSSC encompassing flower shaped assembly of Na-doped TiO2 nanorods sensitized with extract from petals of Kigelia Africana”, Optik - International Journal for Light and Electron Optics, 2017.

[22] Calogero et al., “Photoelectrochemical solar cell comprising sensitizing anthocyanin dyes and method of preparing same”, Patent US9218914B2, 2015.

[23] Amadi et al., “Creation of Natural Dye Sensitized Solar Cell by Using Nanostructured Titanium Oxide”, Nanoscience and Nanoengineering 3(3): 25-32, 2015.

[24] Singh et al., “Natural Dyes and their Effect on Efficiency of TiO2 based DSSCs: a Comparative Study”, Materials Today: Proceedings, 2112-2122, 2018.

[25] Kay and Grätzel, “Artificial Photosynthesis. 1. Photosensitization of TiO_2 Solar Cells with Chlorophyll Derivatives and Related Natural Porphyrins”, Journal of Physical Chemistry, 1993.

[26] Jasim et al., “Curcumin Dye-Sensitized Solar Cell”, Journal of Energy and Power Engineering 11, 409-416, 2017.

[27] Leyrer et al., “Factor Optimization in the Manufacturing Process of Dye- Sensitized Solar Cells Based on Naturally Extracted Dye from a Maqui and Blackberry Mixture (Aristotelia Chilensis and Rubus Glaucus)”, Journal of Electronic Materials, 2018.

[28] Singh et al., “Performance of fruit extract of Melastoma malabathricum L. as sensitizer in DSSCs”, Apectrochimica Acta Part A: Molecular and Biomolecular Spectroscopy 118, 938-943, 2014.

[29] Tennakone et al., “The photostability of dye-sensitized solid state photovoltaic cells: factors determining the stability of the pigment in a nanoporous n-TiO2/cyanidin/p-CuI cell”, Semiconductors Science Technology 12, 128-132, 1997.

[30] Mazloum-Ardakani et al., “Improving the effective photovoltaic performance in dye-sensitized solar cells using an azobenzenecarboxylic acid-based system”, Heliyon 5, 2019.

[31] Martineau, David, “Dye Solar Cells for Real”, Solaronix SA, 2012.

[32] Armendáriz-Mireles et al., “Photocurrent generation by dye-sensitized solar cells using natural pigments”, Biotechnology and Applied Biochemistry, 2015.

[33] Cherepy et al., “Ultrafast Electron Injection: Implications for a Photoelectrochemical Cell Utilizing an Anthocyanin Dye-Sensitized TiO_2 Nanocrystalline Electrode”, Journal of Physical Chemistry, 9342-9351, 1997.

[34] Solaronix, “Ti-Nanoxide T/SP – Screen-Printing Transparent Nanocrystalline Titanium Dioxide”, Application Note, 2013.

[35] Solaronix, “Platisol T/SP – Platinum Catalyst Precursor Paste”, Application Note, 2013.

[36] Tegape, “Telas de Poliéster Monofilamento”, Catálogo de Produtos, 2020.

[37] Solaronix, “Meltronix, Hot-Melt Sealing Films”, April 16, 2020.

http://solaronix.com/materials/products/meltonix/

[38] Turturica et al., “Thermal Degradation of Plum Anthocyanins: Comparison of Kinetics from Simple to Natural Systems”, Journal of Food Quality, 2018.

[39] Ossila, “Electrical Connection Legs for ITO Glass Substrates”, April 17, 2020.

https://www.ossila.com/products/electrical-connection-legs

[40] Novickovas et al., “Compact Light-Emitting Diode-Based AAA Class Solar Simulator: Design and Application Peculiarities”, IEEE Journal of Photovoltaics, 2015.

[41] Tawfik et al., “Light source selection for a solar simulator for thermal applications: A review”, Renewable and Sustainable Energy Reviews 90, 802-813, 2018.

[42] Yujileds, “High CRI LED Lighting”, March 30, 2020.

https://www.yujiintl.com/high-cri-led-lighting.html

[43] NREL, “Reference Air Mass 1.5 Spectra”, February 14, 2019.

https://www.nrel.gov/grid/solar-resource/spectra-am1.5.html

[44] Shimadzu, “Film-Thichness Measurement”, March 25, 2020.

https://www.shimadzu.com/an/uv/support/uv/ap/film.html

[45] Pliskin and Esch, “Refractive Index of SiO_2 Films Grown on Silicon”, Journal of Applied Physics 36, 1965.

[46] Evtushenko et al., “Optical Properties of TiO2 Thin Films”, 4th International Conference Photonics and Information Optics, Physics Procedia 73, 2015.

[47] Antunes, “Amora-preta: Nova Opção de Cultivo no Brasil”, Ciência Rural 32, 151-158, 2002.

[48] Müller et al., “Anti-inflammatory and antioxidant activities of aqueous extract of Cecropia glaziovii leaves”, Journal of Ethnopharmacology, 2016.

[49] The William & Lynda Steere Herbarium, “Cecropia glaziovii Snethl”, April 20, 2020.

http://sweetgum.nybg.org/science/world-flora/monographs-details/?irn=19184

[50] International Coffee Association, “About Coffee – Aspectos Botânicos”, April 20, 2020.

http://www.ico.org/pt/botanical_p.asp

[51] Bote and Struik, “Effects of shade on growth, production and quality of coffee (Coffea arabica) in Ethiopia”, Journal of Horticulture and Forestry 3, 336-341, 2011.

[52] United States Department of Agriculture, “Coffee: World Markets and Trade”, Foreign Agricultural Service, December 2019.

[53] Goldemberg, “The Brazilian biofuels industry”, Biotechnology for Biofuels 1, 2008.

[54] Kalaji et al., “Experimental in vivo measurements of light emission in plants: a perspective dedicated to David Walker”, Photosynthesis Research 114, 69-96, 2012.

[55] Moss and Loomis, “Absorption Spectra of Leaves”, Plant Physiology, 1952.

[56] Soares et al., “Spectrophotometric Determination of Total Sulfite in White Wine Samples Using Crude Extracts from Flowers”, Journal of Chemical Education 79, 2002.

[57] Amcor, “Parafilm® M All-Purpose Laboratory Film”, April 16, 2020.

http://www.bemis.com/na/products/parafilm-floratape/parafilm-lab#

[58] Miranda et al., “Pilidiella tibouchinae sp. nov. associated with foliage blight of Tibouchina granulosa (quaresmeira) in Brazil”, IMA Fungus 3, 1-7, 2012.